

Martian alluvial fans: Comparing fan and catchment areas as a proxy for paleoclimate

Ariana M. Flournoy

A Thesis presented to the Graduate Faculty
of the University of Virginia in Candidacy for the Degree of
Master of Science
Department of Environmental Sciences
University of Virginia
April 22nd, 2024

Committee: Ajay B. Limaye (Chair), Lauren Miller, Kevin Grise

Table of Contents

Acknowledgements	ii
Abstract	iii
1. INTRODUCTION	1
<i>Research questions and hypotheses</i>	1
2. BACKGROUND	2
2.1 <i>Alluvial fans</i>	2
2.2 <i>Applying alluvial fans as a proxy for climate</i>	2
2.3 <i>Alluvial fan morphometry</i>	2
2.4 <i>Martian deposits implicating climate histories</i>	3
2.5 <i>Estimating fan ages on Mars</i>	4
3. METHODS	5
3.1 <i>Temporal and spatial controls on the ratio of fan versus catchment area</i>	5
3.2 <i>Relating the ratio of fan versus catchment area to basin geometry and relief</i>	6
4. RESULTS	7
4.1 <i>Temporal controls on the ratio between fan area and catchment area</i>	7
4.2 <i>Spatial controls on the ratio of fan area versus catchment area</i>	7
4.3 <i>The effects of basin geometry on the ratio of fan area versus catchment area</i>	9
4.4 <i>The effects of catchment relief on the ratio of fan area versus catchment area</i>	10
5. DISCUSSION	11
5.1 <i>Fan age scaling relationship variation</i>	11
5.2 <i>Planetary-scale and local geomorphic setting variation</i>	12
5.3 <i>Basin geometry implications on the ratio of fan area versus catchment area</i>	13
5.4 <i>Catchment relief implications on the ratio of fan area versus catchment area</i>	14
6. CONCLUSIONS	14
7. REFERENCES	16
8. FIGURES	19

Acknowledgments

I wanted to take the time to personally thank my advisor and chair on my committee, Dr. Ajay Limaye, for sharing your wisdom and enthusiasm of space. I would also like to express my appreciation to my committee members, Dr. Lauren Miller and Dr. Kevin Grise, for taking the time to listen to my presentations and offer extremely helpful advice, even when their background knowledge of Mars was minimal. To Dr. Lauren Miller, thank you from the bottom of my heart for being a sounding board for anything I had to say and for believing in my ambition to be and do better. I am eternally grateful to Dr. Brady Foreman for being my undergraduate advisor for 3 years and for making geosciences enjoyable. I am grateful that you have allowed me to bring my interest of planetary science into your office in 2019. Without you I would not have known what to do with my life after graduating, nor would I have dipped my toes into research to place me where I am today.

Special thanks to Paola Granados, Vidushi Sharma, Yuan Li, and Abigail Ackerman for helping me in tough times, reading the many words of my endless rounds of drafts, and for helping me when I was clueless to MATLAB. Without you all, I would not be completely sane. Thank you for also listening to me talk endlessly in the office for the last 2 years. Thank you to the Landscape Evolution Group as well for being a sound board to practice my presentations and for sharing your knowledge of geomorphology. I have enjoyed hearing about every research topic and enjoyed contributing in every discussion. I would like to acknowledge Dr. Marion McKenzie for offering advice on how to survive graduate school, Charlottesville, and teaching. I am very thankful to have known you and to have been welcomed to the University of Virginia by you. You have truly made my experience here fantastic, and I wish more people were as welcoming and as kind as you.

I would be remiss if I did not mention my loving family. To my mom and dad, your educational journey has been the reason I have pushed myself every day and challenged myself intellectually. Thank you for supporting my dreams. I hope I made you all proud. To Jalen and Andrew, I hope my journey serves as an inspiration for you, encouraging you to always pursue your dreams and never give up. You can do anything. Thank you to Jasmine Carmel for being the little window on my screen when I needed someone to hold me accountable to do my work. Thank you for your 8 years of friendship and laughter. Thank you for supporting my aspirations in life and for never allowing me to think small. I have seen you hard at work to achieve your dreams and I am so grateful to know a woman like you who never stops fighting for her passions.

Lastly, I would like to thank my loving partner Lloyd Branch Jr. for supporting me on this endeavor. Without you, I probably wouldn't have had the courage to apply or even attend graduate school. Thank you for investing in my education by paying for every single one of my application fees because you believed in me. Thank you for forcing me to be better every single day and for teaching me patience and confidence. Thank you for always listening to my presentations even if you had no clue what was going on. Lastly, thank you for being such a calm presence during my anxious storms and for reminding me that life is precious and that I should have fun while I can. I appreciate you endlessly and I love you dearly. Thank you.

Abstract

Alluvial fans, formed by fluvial processes or mass wasting events, have been used to interpret paleoclimate, most often using the ratio of fan area to the area of its catchment that provides water and sediment. The recent discovery of alluvial fans on Mars contributes to evidence of previous water flow and one or more major climate transitions that led to the planet's current hyper-arid climate. A recently compiled database (Morgan et al., 2022) cataloged 1,501 alluvial fans globally, and showed a systematic difference in the scaling relationship between fan area and catchment area for cases in impact craters compared to those outside craters. This study tests the hypotheses that 1) scaling relationships between fan and catchment areas vary systematically with crater age and latitude; and 2) observed differences in fan-catchment scaling relationships for craters versus non-craters arise due to differences in basin geometry and catchment relief. To test these hypotheses, I analyzed subsets of alluvial fans and catchments within the global database and fit power-law relationships in the form $A_{fan} = c_1 A_{catchment}^n$. This analysis revealed that 424 alluvial fans in non-craters in the dichotomy boundary ($n_{fans} = 102$) and southern highlands ($n_{fans} = 211$), as well as in Noachian-aged craters ($n_{fans} = 111$), display low exponent values suggesting a weak relationship between catchment area and fan area. In contrast, 1,177 fans formed during the Hesperian ($n_{fans} = 83$) and Amazonian ($n_{fans} = 25$) periods, and in fans hosted within craters ($n_{fans} = 1,069$), exhibit high exponents that suggest a more direct relationship between fan area and catchment area. Subsequently, I considered 5 pairs of study sites with the same catchment area to assess controls on their differing fan areas. The approach for inferring basin geometry using topographic profiles failed for 3/10 cases, suggesting that an alternative geophysical approach would be needed. However, for these case studies, catchment relief was lower for fans in craters, which may explain why fan scaling relationships between fan area and catchment area are consistently different for craters versus non-craters at a global scale. These analyses suggest that the age of the fan, geographic location, and the geomorphic setting (crater versus non-crater) are important context for interpreting the scaling relationship between fan area and catchment area on Mars. To place further constraints on the Martian paleoclimate, future research is necessary to discern whether differences in fan geometry were the result of geologic conditions (e.g., basin geometry) versus differences in climate.

1. Introduction

Alluvial fans are depositional landforms created by mass transport of sediment from high to low slope. As water interacts with the surface several geomorphic processes can construct alluvial fans including sheetfloods, debris flows and landslides (Blair & McPherson, 1994). The sediment deposited during these events originates from the upstream catchment (Bull, 1977; Giles, 2010). Alluvial fans on Earth are found in arid, glacial, and humid environments and have been used to infer important paleoclimate changes over millennial timescales (Dorn, 1994). For example, grain size trends on alluvial fans have been used to interpret paleoclimate changes based on differing modes of sediment transport under glacial and periglacial climates (D'Arcy et al., 2017). Perhaps the most common approach to interpreting paleoclimate from alluvial fans involves their planform geometry: the ratio between fan area to catchment area has been widely serve as a proxy for erosional efficiency in the catchment (Giles, 2010; Harvey, 1997a; Stock, 2013).

Currently, Mars is a dry and uninhabitable planet generally with basalt-rich landscapes and widespread impact craters. Previously, the Martian climate was warm and wet, but it is still unknown how it transitioned to a cold and arid state (Kite, 2019; Wordsworth, 2016). Evidence for a wetter past climate states includes large, fan-shaped deposits revealed in satellite images and topography data (Jakosky, 2021; Malin et al., 2007; Mondro et al., 2023; Moore, 2005; Morgan et al., 2022; Wilson et al., 2021). The deposits were interpreted to be alluvial fans and are often located within craters in the southern highlands, near the dichotomy boundary, as well as near valley networks (Hynek et al., 2010; Jakosky, 2021; Moore, 2005; Morgan et al., 2022; Robbins & Hynek, 2012; Wilson et al., 2021). Morgan et al. (2022) recently produced a comprehensive global map of alluvial fans revealing distinct catchment scaling relationships for fans within craters and those outside of craters. Because alluvial fans imply past periods when water was stable at the surface, they are crucial landforms for constraining past climate conditions on Mars (Jakosky, 2021; Kite, 2019; Moore, 2005; Morgan et al., 2022; Wilson et al., 2021; Wordsworth, 2016). This work builds on the mapping and interpretations of Morgan et al. (2022) to test for spatial and temporal trends in the geometries of alluvial fans and their associated catchments. I seek to address two questions: 1) do differences in scaling relationships between alluvial fans and their catchments imply paleoclimate differences in space and/or time? I hypothesize that the ratio of fan to catchment area varies systematically with fan age and latitude. To test this hypothesis, I will recalculate scaling relationships using subsets of observations from the Morgan et al. (2022) database based on planetary-scale geomorphic setting and fan age. The second question is: why does the scaling relationship between fan area and catchment area vary for craters versus non-craters? I hypothesize that these differences arise because of systematic differences in catchment geometry and relief between craters and non-craters. To test this hypothesis, I will control for catchment area and test whether catchment relief and/or basin geometry vary systematically across 10 study sites (5 fans within craters, 5 outside of craters) from the Morgan et al. (2022) global database.

Research Questions and Hypotheses

- ◆ Q1: Does the ratio of alluvial fan area to catchment area imply paleoclimate differences in space and/or time?

H1: I hypothesize that the ratio of fan to catchment area varies systematically with fan age, latitude, and geomorphic setting.

- ◆ Q2: Why does the ratio of fan area to catchment area vary for craters and non-craters?

H2: I hypothesize that the ratio of fan area to catchment area vary due to differences in catchment relief and basin geometry, which affects how sediment accumulates on the basin floor.

2. Background

2.1 Alluvial fans

Alluvial fans often form at sharp transitions in topography from high to low slopes. The catchment for an alluvial fan may receive water from either snowmelt or precipitation, causing the sediment to move downslope. The processes that create these fans are either fluvial (i.e., involving flowing water) or are from mass wasting events such as landslides or debris flows. Alluvial fans typically contain large grain sizes, but this can vary depending on the hydrologic processes in which these fans were made, as well as the geologic makeup of the catchment (Blair & McPherson, 1994). Larger grain sizes (boulder and cobble sized) found on the fan allude to a lower erosional efficiency of the catchment and mass wasting events (Blair & McPherson, 1994; Sundararajan et al., 1990). Smaller grain sizes (sand and pebble sized) found on the fan means the catchment has a higher erosional efficiency and fluvial sediment transportation (Blair & McPherson, 1994; Sundararajan et al., 1990). Alluvial fans tend to have different shapes based on the climate due to the type of hydrologic process that influence sediment transport to build the fan such as having a typical conical shape or having more of an elongate irregular shape (Blair & McPherson, 1994; Harvey, 1997; Kochel, 1990; Lecce, 1990; Rachocki & Church, 1990). One of the most studied sites for alluvial fans on Earth is in Death Valley, CA near Badwater Basin (Blair & McPherson, 1994) (Figure 1). The Death Valley fans have been important in studying the fan slopes, deposits, and climatic and tectonic controls on fan formation (Blair & McPherson, 1994).

2.2 Applying alluvial fans as a proxy for paleoclimate

D'Arcy et al. (2017) interpreted grain size trends on alluvial fans to place constraints on the nature of past flow events during spanning glacial-interglacial transitions. Environments with a warm, dry climate tend to transport coarser grained deposits due to having brief, high discharge events caused by with intense rates of precipitation or snowmelt (Chen et al., 2004; D'Arcy et al., 2017). Dissimilarly, environments with cooler, wet glacial climates have been interpreted to transport finer-grained sediment to fans due to lower precipitation or snowmelt rates (Chen et al., 2004; D'Arcy et al., 2017). Compared to fans formed by mostly fluvial processes, those formed primarily by debris flows are more irregular in shape and varied in size (Dorn, 1994; Kochel, 1990). In contrast, fluvially dominated fans have a more conical shape and are typically larger (Dorn, 1994; Kochel, 1990). Research has been done to relate climate to the morphometry of the alluvial fan by measuring the fan shape and area to its corresponding catchment area in arid and humid environments (Dorn, 1994; Giles, 2010; Harvey, 1997a; Stock, 2013).

2.3 Alluvial fan morphometry

Alluvial fans are closely associated with the catchments that supply water and sediment. Therefore, it is common to measure the area of the fan and the area of the catchment, and relate the two using a power law:

$$A_{fan} = c_1 A_{drainage}^n \quad (1)$$

where A_{fan} is fan area, $A_{drainage}$ is catchment drainage area, and c and n are dimensionless, fitted parameters (Stock, 2013). The value of c is a proxy for cumulative sediment transport from the catchment, as larger values of c correspond to larger fans for small catchment areas (Harvey, 1997;

Stock, 2013). The value of n describes the strength of the relationship and reflects the idea that larger catchment areas produce similarly larger fan areas (Giles, 2010) (Figure 2).

Fan morphometry relates to the relative erodibility of the catchment and the efficiency of sediment transport (Bull, 1977; Stock, 2013). Catchments that have high erosion rates and transport rates have proportionally larger fan areas (Bull, 1977; Giles, 2010; Harvey, 1997; Stock, 2013). The ratio of fan area to catchment area is therefore relevant for interpreting previous discharge and sediment dynamics within the catchment at the time of fan of fan formation (Bull, 1977; Giles, 2010).

2.4 Martian deposits implicating climate histories

Mars has many physical differences compared to Earth such as: not having plate tectonics; having less varied geology on the surface; no liquid water on the surface; lower gravity, and having a consistent dichotomy in mean elevation and crustal thickness between the north and south hemispheres (Robinson, 1995; Wordsworth, 2016). The northern part of Mars has an average elevation of ~ 5 km lower than the southern highlands and has a crustal thickness between 30-40 km (Pan et al., 2017). Comparatively, the southern highlands contain an average elevation of approximately 2 km with a crustal thickness between 70-80 km. Notable geologic features of the southern highlands include Hellas basin, a major impact basin; the Tharsis bulge, a broad volcanic rise; and Valles Marineris, the largest canyon in the solar system. The dichotomy boundary is a region that contains intermediate elevation between the north and the south (Figure 3). It lies on the edge of the Valles Marineris and north the Olympus Mons, the main volcano in the Tharsis bulge.

The history of water on Mars has been a long-studied question that has yet to be fully answered. Partial pieces of the story of water on Mars have been investigated for the last 50 years using satellite data. Topographic data have been used to see large differences in elevation on landscapes by utilizing the Mars Orbiter Laser Altimeter (MOLA) onboard the Mars Global Surveyor (MGS) (Smith et al., 1999). Mineral and rock types have also been inferred from imaging spectrometers and instruments such as the Thermal Emission Imaging System (THEMIS) (Christensen et al., 2004). These remote sensing observations, combined with rover data, have revealed the stratigraphy of craters (such as Gale crater) including clay and sulfate minerals along the northern part of the southern highlands (Milliken et al., 2010).

Fluvial features, such as sinuous channel bodies and valley networks, indicate a wetter Martian climate around the Noachian period (~ 4.6 -3.5 Gya) (Moore et al., 2003). Moore et al. (2005) had explored 31 large fans found within craters and determined a scaling relationship relating fan and catchment area using the Harvey et al. (1987) power law. They found that Martian alluvial fans have a similar trend of fan area to catchment area as terrestrial alluvial fans studied by Harvey et al. (1997).

Morgan et al. (2022) used previous databases of fan shaped deposits to create a global distribution map of 1,501 fans found on the surface of Mars (Di Achille & Hynek, 2010; Grant & Wilson, 2011; Hynek et al., 2010; Moore, 2005; Robbins & Hynek, 2012; Wilson et al., 2021). They characterized the fans based on their overall shape and terrestrial interpretation such as alluvial fans, smooth scarp fronted deposits (SFDs), channelized SFDs, and terraced SFDs. They gathered information such as fan slope gradient, directionality, fan area, catchment area, and fan elevation and related these measurements to latitude and fan age to place better constraints on the climate on Mars. Their work showed that by using Equation 1, the power law trend found for Martian fans located in different geomorphic settings, such as within craters and non-craters, the

exponent n , was larger for fans in craters than fans in non-craters. They also found that the proportionality constant, c , for fans in craters was smaller than the proportionality constant for fans in non-craters. Their work provided evidence to support that the global Martian trend between fan and catchment area was comparative to the trend found for terrestrial alluvial fans (Figure 4). More specifically, many fans were found to have a similar trend to fans found in Fresno County, CA (Bull, 1963). The Fresno County alluvial fans were formed from mudflow events and the fan stratigraphy in Saheki crater (21.75°S, 286.97°W) suggests that they were created by mudflow events (Morgan et al., 2014). Morgan et al. (2022) distinguished that these fans were potentially created under snowmelt or precipitation conditions that were episodic. This answer was determined by examining potential sources of runoff that can drive alluvial fan formation and exploring which source would be likely under interpreted time constraints. They deemed that a snowmelt interpretation is more supported than precipitation conditions by the lack of fluvial activity found within fan-hosting craters aside from the activity found on the fan (Grant & Wilson, 2011; Moore, 2005).

2.5 Estimating fan ages on Mars

The Noachian period began 4.5 Ga, ended 3.5 Ga, and coincides with a wet and warm climate as well as heavy cratering occurring on the surface (Kite, 2019; Wordsworth, 2016). During the early Noachian period, the crust of Mars was formed, and large impact basins were formed such as Hellas Basin. During the late Noachian period, evidence has been found to infer that the climate on Mars was wet and warm enough to form fluvial based landforms such as deltas, alluvial fans, and channels. The Hesperian period began 3.5 Ga to 3.0 Ga and is linked to heavy volcanic events such as the formation of Tharsis Bulge, as well as catastrophic flooding events creating valley networks potentially from the continuous volcanic eruptions introducing greenhouse gases and volcanic particles into the dense CO_2 Martian atmosphere at the time of formation. The Amazonian period began 3.0 Ga and is known as present day Mars. This period is associated with hyper-arid conditions, an extremely thin CO_2 atmosphere, and minimal weathering events.

Previous work has been done by Holo et al. (2021), Kite et al. (2017), Morgan et al. (2022), Tanaka et al. (2014), and Wilson et al. (2021) to estimate surface ages on Mars. One of the main ways to gather surface ages is to utilize impact craters to determine old versus new surfaces. Older surfaces will tend to have more craters and younger surfaces will be smoother and have a smaller density of impact craters. These observations are gathered in isochron plots like those by Hartmann (2005), which are used to estimate surface ages by obtaining the crater density in a study region and the diameters of each crater in that region. Tanaka et al. (2014) created an updated geologic unit map of Mars that synthesizes patterns in surface age at large scale. Tanaka et al. (2014)'s global geologic map of Mars shows chronostratigraphic ages, topographic and crater characteristics, as well as resurfacing history. They gathered surface ages by utilizing stratigraphic relations and crater density counting. Their crater counting methods were similar to the methods used by Holo et al. (2021) by using the Craterstats software tool (Michael & Neukum, 2010). They also approached gathering crater counting results by using the Robbins & Hynek (2012) crater database. The units on the geologic map were then recorded to be placed in the Martian periods (Noachian, Hesperian, and Amazonian) and subdivided into eight epochs (early, middle, late Noachian; early and late Hesperian; early, middle, late Amazonian).

Many alluvial fan ages have been traced to periods as recent as the Hesperian to late Amazonian (2000 Ma-present) by using the crater database and chronostratigraphic age map (Grant & Wilson, 2011; Holo et al., 2021; Kite et al., 2017; Tanaka et al., 2014). One interpretation based on these

analyses is that Martian fans were formed over multiple years rather than a singular catastrophic event and that the location in which these fans occur may relate potential climate variations in the past (Moore et al., 2005). For example, these fans have been argued to record a plausible river-supporting climate on Mars during the Early to Late Hesperian (<3.5Ga) (Figure 5) (Kite et al., 2017; Moore, 2005) allowing for a discharge of about $10^2 \text{ m}^3/\text{s}$, which is consistent with precipitation runoff, based on the amount of sediment moved (Dietrich et al., 2017; Kite et al., 2017). Holo et al. (2021) used statistical analysis by Michael et al. (2016) to determine fan ages for fans located in the Amazonian-Hesperian Impact Unit (AHi) subunit found by Tanaka et al. (2014). Holo et al. (2021) found that the fans were likely to have been formed during the Amazonian period (~2.5 Gyr) and their estimate is about 1 billion years earlier than previously estimated by other researchers (Figure 5) (Grant & Wilson, 2011; Moore et al., 2003; Wordsworth, 2016). Similarly, Morgan et al. (2022) also investigated the fan surface ages but used different methods to gather them. Morgan et al. (2022) gathered maximum surface ages by looking into the fan-hosting crater ejecta to find the host crater ages to set a maximum surface age for fans and found similar fan surface age maximums as Holo et al. (2022).

3. Methods

I developed a script to extract morphometric data for each fan from the dataset compiled by Morgan et al. (2022), aiming to investigate temporal and spatial influences on the fan area to catchment area ratio. The script was designed to generate plots of fan area against catchment area for various subsets of the dataset. The first set of analyses examined temporal controls, relying on crater-based fan age information provided by Morgan et al. (2022) and was divided into subsets such as: Noachian-aged craters, Hesperian-aged craters, and Amazonian-aged craters. The second set of analyses examined several subsets to isolate the fan area and catchment area based on fan location via latitude and geomorphic setting and was then divided into subsets such as: northern lowland located fans, fans found within the dichotomy boundary in craters and non-craters, and fans located in the southern highlands within craters and non-cratered boundaries.

3.1 Temporal and spatial controls on the ratio of fan versus catchment area

To explore temporal controls, subsets of alluvial fans within craters were delineated using the crater age data from the Morgan et al. (2022) database. The objective of the investigation is to assess the impact on the scaling relationship between fan area and catchment area. Although the Morgan et al. (2022) database provided ages for both fans and their host craters, only crater ages were utilized for fan age subsets to maintain data consistency for this study. Crater-based fan ages were gathered for only $n = 219$ fans out of the entire database (Kite et al., 2017; Morgan et al., 2022; Wordsworth, 2016). Each subset was then plotted on scatter plots organized by geologic time periods, revealing new systematic variations between fan area and catchment area.

To understand how spatial controls affect the scaling relationship between fan area and catchment area, latitude subsets were chosen based on the Martian dichotomy boundaries. I referenced the Morgan et al. (2022) dataset for catchment area and fan area values. Utilizing ArcGIS Pro, I delineated boundaries between the northern lowlands, dichotomy boundary, and southern highlands, integrating these divisions into the script. Latitude boundaries were established by consulting the MOLA Digital Elevation Model (DEM) global map, which featured colorized elevation data to distinguish elevation levels on Mars. Additional verification of boundaries was conducted using external sources including JMARS. The delineated boundaries were used to

determine which alluvial fans from the Morgan et al. (2022) database was found within each boundary and whether they were found in craters or in non-craters. After the subsets of alluvial fans were gathered, five scatter plots were created based on each latitudinal boundary and whether the alluvial fans were found within craters or outside of craters to fit a new scaling relationship for subsets of the data.

3.2 Relating ratio of fan versus catchment area to basin geometry and catchment relief

Building upon the research conducted by Morgan et al. (2022), I extended the investigation to test the variations in the ratio between fan area and catchment area for alluvial fans within and outside craters (Figures 3b, 4a, 4b). The goal was to test for systematic differences in fan geometry that could be caused by geomorphic settings. To achieve this, I selected five pairs, each consisting of one fan within a crater and one outside of a crater, amounting to ten fan and catchment points from the Morgan et al. (2022) database. Pair selection was based on similar catchment areas within each pair to examine whether the geomorphic setting influences catchment and fan sizes. I hypothesize that the fan geometry heavily relies on basin geometry and how steep the catchment itself is (Figure 6).

Upon determining the pairs, I used ArcGIS Pro to map these points onto the MOLA DEM global map, illustrating variations in elevation at these locations (Figure 7). Initial validation involved confirming the catchment relief of the ten shapefiles against the relief measurements provided by the Morgan et al. (2022) database, ensuring the accuracy of catchment boundaries. This validation process utilized a script to extract relief values from the global MOLA DEM. To investigate if catchment relief causes a systematic variation between fans found within craters and fans outside of craters, the catchment relief from the Morgan et al. (2022) database for each study site was plotted against the fan area for five separate scatter plot graphs. The graphs were aligned by increasing catchment area from left to right.

Table 1. Five pairs from 10 study sites (Figure 3a) chosen from the Morgan et al. (2022) database showing the fan area, catchment area, and its respective geomorphic setting. Each pair was selected to compare fans with similar catchment areas, with one fan located within a crater and the other outside a crater.

Pair number	Geomorphic Setting	Catchment Area (km^2)	Fan Area (km^2)
1	Within a crater	2.82	1.04
	Non-crater	2.74	1.33
2	Within a crater	21.96	6.31
	Non-crater	21.42	8.96
3	Within a crater	81.74	27.84
	Non-crater	78.97	153.67
4	Within a crater	144.32	7.72
	Non-crater	141.59	43.23
5	Within a crater	10,066.8	574.1
	Non-crater	9,623.01	212.60

Following catchment boundary validation, elevation profiles for each study site catchment were generated to investigate potential systematic differences in catchment topography between craters and non-craters. On fan profile lines were placed at the end of the catchment to the end of the fan to understand how the fan is built within the basin. To gather the basin geometry adjacent

to the fan, profile lines were marked away from the fan to ensure the line was not touching a coalescing fan. This was done to each pair of fans for all 10 case study sites. Longitudinal profiles were made by interpolating points along the profile onto the MOLA DEM dataset to gather elevation differences and the distance between A to A' along the fan or B to B' for profiles adjacent to the fan.

4. Results

4.1 Temporal controls on the ratio between fan area and catchment area

Figure 8 depicts a plot of fan area against catchment area for three fan subsets: Noachian-aged, Hesperian-aged, and Amazonian-aged fans. A total of 219 fans from the original dataset were included in the plot, with the limitation arising from constraints associated with crater counting, as outlined by Morgan et al. (2022). The fan ages discovered rely on the ages of the craters in which the fans are situated. Each subset is accompanied by a trendline illustrating the overall fan area to catchment area scaling relationship. The study identified a total of $n_{fans} = 111$ Noachian-aged fans (Figure 8a), as detailed by Morgan et al. (2022). Additionally, $n_{fans} = 83$ Hesperian-aged fans (Figure 8b) were cataloged using the Morgan et al. (2022) database, while $n_{fans} = 25$ Amazonian-aged fans (Figure 8c) were identified by the same source. Each temporal subset has gathered a power law trend to explain the relationship between fan area and catchment area. The first value explains the proportionality constant of the relationship and the exponent explains the scaling relationship between the fan area and catchment area and the likelihood for a large catchment to form an equally large fan.

For Noachian aged fans ($n_{fans} = 111$), three alluvial fans were found with a catchment area exceeding 150 km^2 and a fan area less than 35 km^2 , highlighting instances where larger catchment sizes do not necessarily correlate with proportionately larger fan sizes and sediment flux. However, most Noachian-aged fans featured catchment sizes ranging from 3 km^2 to 75 km^2 , coupled with fan areas between 1 km^2 and 50 km^2 . The statistical power law found is $A_f = 2.82 * A_c^{0.53}$ (Figure 8a). This scaling relationship shows a square root correspondence between catchment area and fan area, noting that catchment area is a weak indicator for fan area.

Hesperian aged alluvial fans ($n_{fans} = 83$) have a statistical power law relationship of $A_f = 1.52 * A_c^{0.80}$ (Figure 8b). The alluvial fans within Hesperian aged craters have a catchment area to fan area relationship that is evenly distributed with 1 singular outlier that has a catchment area of 1190 km^2 with a fan area of 30 km^2 . The rest of the alluvial fans fall within a range of catchment areas between 1 km^2 and 170 km^2 with corresponding fan areas between 1 km^2 and 300 km^2 .

Alluvial fans formed within Amazonian aged craters ($n_{fans} = 25$) show widespread distribution (Figure 8c). 2 outliers exist on the lower end of the trend showing a fan with a catchment area of 1.5 km^2 and fan area of 9.8 km^2 and another fan with a catchment area of 3.7 km^2 with a fan area of 0.9 km^2 . Amazonian aged alluvial fans have a statistical power law relationship of $A_f = 0.92 * A_c^{0.97}$ resulting in having an almost linear correlation. This shows that catchment area is a strong indicator for fan area.

4.2 Spatial controls on the ratio of fan area versus catchment area

A distinct elevation contrast on the Martian surface occurs between its northern and southern hemispheres. The northern hemisphere exhibits a relatively low elevation, approximately -4 (on average) km, while the southern hemisphere showcases higher elevations ranging from 0 km to 4 km (and beyond that for the Tharsis bulge). This elevation dichotomy is further emphasized by

substantial cratering on the southern hemisphere, contrasting with the relatively smoother terrain observed in the northern hemisphere. The demarcation between these contrasting features is delineated by the Martian dichotomy boundary. Alluvial fans noted by Morgan et al. (2022) have been found globally within craters and non-craters (such as along valley walls and down volcanic slopes). For fans found in craters globally, Morgan et al. (2022) noted that the scaling relationship was $A_f = 1.27 * A_c^{0.97}$ (Figure 4). For alluvial fans found outside of craters globally, Morgan et al. (2022) discovered a scaling relationship of $A_f = 5.37 * A_c^{0.50}$ (Figure 4).

Within the northern lowlands, 97 alluvial fans were found. Of the 97 fans found, $n_{fans} = 96$ was located within a cratered geomorphic setting, and $n_{fans} = 1$ was found within a non-cratered geomorphic setting. A new scaling relationship was found for fans located within craters in the northern lowland boundary: $A_f = 0.99 * A_c^{0.97}$ (Figure 9a). The exponent, 0.97, shows an almost linear relationship noting that catchment area is a good indicator for fan area for this latitude boundary. The scaling relationship is also relatively close to the one found by Morgan et al. (2022) globally for in crater geomorphic settings (Figure 4). The scatter of the alluvial fans was found to vary, but a cluster of fans were determined to have a catchment area between 1 km² and 90 km² with fan areas ranging from 1 km² to 180 km². An outlier was found to have a catchment area of 393 km² with a fan area of 14.7 km². For the single fan found in a non-crater within this boundary, the catchment area was 283 km² with a fan area of 62.8 km². This subset was not examined due to the inability to examine a scaling relationship for 1 singular point.

338 alluvial fans were found in the dichotomy boundary with $n_{fans} = 236$ fans found inside of a cratered geomorphic setting, and $n_{fans} = 102$ within a non-cratered geomorphic setting. 236 alluvial fans within craters in this boundary had a new scaling relationship of $A_f = 1.90 * A_c^{0.68}$ (Figure 9b). Many of the alluvial fans within this boundary in craters have a catchment area between 1 km² and 150 km² with a corresponding fan area between 1 km² and 120 km². 102 alluvial fans in a non-cratered geomorphic setting within this boundary had a scaling relationship of: $A_f = 5.98 * A_c^{0.42}$ (Figure 9c). A large cluster of fans in this non-cratered geomorphic setting occurs above the trendline and were found to have a catchment area between 5 km² and 25 km² with a fan area between 4 km² and 65 km².

For alluvial fans within the southern highland latitude boundary, a total of $n_{fans} = 947$ fans were found. 736 alluvial fans were discovered within a cratered geomorphic setting with a new scaling relationship of: $A_f = 1.45 * A_c^{0.76}$ (Figure 9d). A tight cluster of alluvial fans was found to have a catchment area between 1 km² and 215 km² with a fan area between 1 km² and 550 km². For a non-cratered geomorphic setting, $n = 211$ alluvial fans were found, and the scaling relationship of these fans was: $A_f = 5.37 * A_c^{0.50}$ (Figure 9e). Many of the alluvial fans within this setting were found to have a catchment area between ~3 km² and ~100 km² with a corresponding fan area between 3 km² and ~140 km².

In summary, the relationship between fan area and catchment area is notably stronger for alluvial fans formed within cratered geomorphic settings in the northern lowlands shown by the exponent of 0.97. Similarly, alluvial fans formed in craters in the southern highlands and dichotomy boundary exhibit a higher exponent (> 0.6) with a relatively low proportionality constant (< 2) corresponding with the original global in-crater values found by Morgan et al. (2022). Contrarily, alluvial fans formed in non-cratered settings geographically display a weaker correlation, nearing 0.50, indicative of a square-rooted relationship between fan area and catchment area. The proportionality constant for alluvial fans in non-cratered settings in the

dichotomy boundary and southern highlands exhibit high values that is comparable to the original out of crater global values found by Morgan et al. (2022).

4.3 The effects of basin geometry on the ratio between fan area and catchment area

The relationship between catchment area and fan area for alluvial fans may depend on the basin in which the fan is formed in and the overlying structure and elevation of the catchment itself. I hypothesize that for the fans built in craters, both the fan surface and the basin floor will contain a steeper slope and that for non-cratered settings, both fans and basin floors will have gentler slopes allowing for the fan to outstretch, causing the fan area to be larger for fans in non-cratered scenarios (Figure 6). To test how the basin geometry affects the ratio between fan area and catchment area, I gathered topographic profiles along the fan and within the basin adjacent to the fan. I chose 10 study sites that had similar catchment areas with differing fan areas under 2 geomorphic settings (in crater and non-crater) (Table 1, Figure 3a, Figure 6). The profile on the fan was gathered at the apex of the fan to the front of the fan to understand the geometry of the fan and another profile was taken adjacent to the fan to understand the geometry of the basin in which the fan was formed. Each crater and non-crater study site was named using the identifiers created by Morgan et al. (2022).

Pair 1 (Table 1, Figure 10) shows a map view of the in crater and non-crater study sites. The profile on the fan in Crater 15-1-37943-12 from A-A' shows a steep and almost linear slope (Figure 10c). The profile of the basin adjacent to the fan from B-B' shows a steep slope as well with a general concave geometry signifying the typical bowl shape of the crater (Figure 10c). However, for the non-crater scenario in MC-23-5, the model approach has failed due to the basin profile exhibiting a higher elevation than the profile of the fan throughout, potentially due to the low resolution of the DEM (Figure 10d). This pair shows that the slope of the fan profile in the crater is steeper than the fan in the non-crater scenario, consistent with my hypothesis (Figure 6).

In pair 2, the fan's respective catchment in Crater 14-1-02218-1 exhibits a sinuous shape (Figure 11a). When examining the fan's profile from A-A' within the crater, a typical concave shape is evident, featuring a steep slope near the apex that gradually diminishes towards the fan's terminus. The profile of the basin adjacent to the fan from B-B' has an elevation that is lower than the fan by about 50 m and displays a concave shape for the crater (Figure 11c). The non-crater scenario of the profile on the fan exhibits a gentle slope compared to the in-crater scenario. The profile of the basin adjacent to the fan from B-B' shows a steep slope along the escarpment (Figure 11d). The fan within the crater exhibits a steeper slope compared to the fan in the non-crater scenario which aligns with my hypothesis (Figure 6).

In pair 3, the examination of the alluvial fan within Crater 11-0-00122-2 highlights a failure within the model approach. As depicted in Figure 12c, the basin profile contains a higher elevation than the fan profile throughout. This failure could stem from the limitations of the data due to the low resolution of the elevation model, or possibly from the basin profile being taken on a coalescing fan. The fan and basin profile in non-crater MC-18-6 displays a concave shape where the basin has a steeper slope than the fan (Figure 12d).

Both alluvial fans in pair 4 exhibit variable profile curvatures. The fan in Crater 11-0-033065 exhibits an almost linear profile that transitions to a gentle convex slope and the slope of the fan in MC-0-91 is steep and displays an elevation shift towards the middle of the fan (Figure 13). The fan in MC-0-91 is located at the bottom of a volcano near the Tharsis Bulge and contains a long sinuous catchment (Figure 13b). The basin profile for MC-0-91 displays a relatively linear and steep slope from 0 to ~1000 m that becomes convex (Figure 13d). This change in profile may be

due to the B-B' profile being examined on a potential deposit. Given that the profile of the fan in MC-0-91 has a steeper slope than the fan in Crater 11-0-033065, this pair does not match my hypothesis (Figure 6).

Lastly, in pair 5, the profile of the fan in Crater 10-0-120391 from A-A' exhibits a convex shape, whereas the basin shows a very steep concave profile (Figure 14c). The non-crater scenario in MC-13-4 shows a potential failure in the model approach given that the profile of the fan from A-A' generally has a low elevation in comparison to the basin profile from B-B' (Figure 14d). This may be due to the location in which the profile was taken. Furthermore, due to the steeper gradient of the fan in the crater than the fan in the non-crater scenario, this pair shows consistent results with my hypothesis (Figure 6).

In summary, the analysis of five pairs reveals mixed outcomes. In three of the five pairs examined the alluvial fans in the crater scenarios display a steeper fan profile than the respective non-crater scenario (Figure 10, Figure 11, Figure 14). Conversely, two of the five pairs of the fans were steeper in the non-crater scenarios (Figure 12, Figure 13). Importantly, the approach for estimating the profiles of the buried basin floor was unsuccessful in three out of the 10 cases because the estimated basin profile was higher in elevation than the fan profile. Therefore, the results for fan profiles are more reliable than for basin profiles.

4.4 The effects of catchment relief on the ratio between fan area and catchment area

Using the 10 study sites listed above (Table 1, Figure 3a), I tested how the catchment relief can affect the ratio between fan area and catchment area. I utilized the Morgan et al. (2022) database to gather the catchment relief for each catchment study site. Following this, five scatter plots were made to determine a trend between catchment relief and fan area for fans formed within craters and those formed in non-craters. The plots are put in ascending order with the catchment area increasing over the five plots and pairs (Figure 15).

For pair 1, the fan in the crater had a catchment relief of 0.55 km with a corresponding fan area of 1.04 km². In comparison to this, the fan located in a non-crater with a similar catchment area had a catchment relief of 0.42 km and a fan area of 1.33 km². Between the two sites in this pair, there is no apparent effect on catchment area from catchment relief alone given that the relief and fan area of both sites are very similar.

Pair 2 has a better variation between the catchment relief for the fans in crater and non-crater. For the fan within the crater, the catchment relief was 0.84 km, and the fan area is 243.5 km². The catchment relief for the study site in the non-crater was 2.18 km and its corresponding fan area is 15.1 km². This shows that the fan within the crater that has a smaller catchment relief has a relatively larger fan area in comparison to the fan in the non-crater with a larger catchment relief with a smaller fan area.

The fan in the crater for pair 3 has a catchment relief of 1.62 km with a fan area of 8.7 km². The catchment relief for the fan in the non-crater is 3.04 km with a fan area of 128.3 km². For this pair, the fan within the crater has a low catchment relief with a similarly small fan, and the fan in the non-crater has high relief in the catchment producing a respectively larger fan.

For pair 4, the fan within the crater has a catchment relief of 1.68 km with a fan area of 523.9 km². The fan found in the non-crater has a catchment relief of 5.15 km with a fan area of 59.01 km². The in-crater fan has a low relief in the catchment that produces a large fan whereas the fan in the non-crater has a higher relief with a relatively low fan area in comparison.

Finally, the 5th pair shows that the in crater alluvial fan has a catchment relief of 0.13 km with a fan area of 55.7 km². The fan in the non-crater has a catchment relief of 2.74 km and a fan area

of 443.6 km². This shows that for this pair, the fan in the crater has a catchment with low relief that produces a similarly small fan. The fan in the non-crater has a relatively higher relief than the fan in the crater that produces a large fan. Throughout this analysis, 4 of the 5 study cases worked showing that catchment relief is generally low for fans located in craters than fans in non-craters.

5. Discussion

The ratio of alluvial fan area to catchment area has been previously studied extensively on Earth (A. Harvey, 1990; Adrian Harvey, 1997a; Moore, 2005; Morgan et al., 2022). Recent literature suggests that variations in this ratio occurs for fans located within craters on Mars and in non-craters, such as along the dichotomy boundary and within Valles Marineris (Morgan et al., 2022). The objective for this analysis was to understand why this variation exists by looking at two factors that control the variation such as basin geometry and catchment relief. Another objective for this analysis was to look for a systematic variation between fans found in different latitudes and during different geological periods on Mars to place better constraints on the climate at the time of alluvial fan formation. To complete this, I used the Morgan et al. (2022) alluvial fan database to compare my new scaling relationships to their original varying relationships between fans in different geomorphic settings (Figure 4).

5.1 Fan age scaling relationship variation

Mars contains an extensive geologic history shaped by 3 major periods. The first of which is the Noachian period and was widely known for surfaces being heavily impacted. It is also recognized for having a warm and wet climate towards the end of the period. As a result of this, loose sediment is sustained at the rim of craters that can be transported downslope to build alluvial fans. 111 alluvial fans have been recorded to be hosted within Noachian-aged craters by Morgan et al. (2022). The new scaling relationship for Noachian-aged fan area versus catchment area is $A_f = 2.82 * A_c^{0.53}$ (Figure 8a). Compared to the original scaling law for fans within craters: $A_f = 1.27 * A_c^{0.97}$ (Morgan et al., 2022), this new relationship shows that the proportionality constant of 2.82 is higher, suggesting that more sediment was transported from the catchment to the basin compared to the full survey of fans within craters over all time periods. This may be due to the loose sediment at the crater rim as well as the warm and wet climate that was previously discussed allowing for more effective sediment transport. The exponent within the scaling relationship between fan area and catchment area, however, has decreased for Noachian-aged fans meaning the catchment area is not directly proportional to creating equally sized fans. Smaller catchment areas are linked to having larger fan areas. This may be interpreted as a climate contributing to mass wasting events causing fan formation rather than fluvial sediment transport, based on interpretations of exponents for terrestrial data (Dorn, 1994; Giles, 2010; Harvey, 1997a).

The Hesperian period began 3.5 Ga and ended 3.0 Ga and consisted of catastrophic flooding events and valley formation. Craters were still forming on the surface, but dissimilar to the Noachian period. 83 alluvial fans were found in Hesperian-aged craters. This value is lower than the amount found in Noachian-aged craters by 75%. The scaling relationship found for this set of alluvial fans is: $A_f = 1.52 * A_c^{0.80}$ (Figure 8b). The proportionality constant (1.52) is closer to the original scaling relationship representing that the estimated climate or erosional efficiency for this period is similar to the average of the two factors. The exponent of the relationship between fan area to catchment area for fans in Hesperian-aged craters is 0.8, alluding to the idea that large catchment areas may produce similarly large fan areas (Figure 8b). This is interpreted to be caused

by fluvial transport events moving sediment from the catchment to the basin creating equally large fan sizes.

The Amazonian period began 3.0 Ga and is the current period. This period is linked to the current hyper-arid climate that contains seasonal dust storm events and has a thin atmosphere. 25 alluvial fans have been discovered in Amazonian-aged craters (Morgan et al., 2022) which is 11% of the total fans investigated in aged craters by Morgan et al. (2022). The new scaling relationship for this subset is $A_f = 0.92 * A_c^{0.97}$ (Figure 8c). The proportionality constant has decreased slightly in comparison to the original total in crater subset scaling relationship from 1.27 to 0.92. This decrease shows that the climate did become drier than the overall averaged climate to move sediment and the erosional efficiency has decreased potentially due to the lack of loose sediment at the crater rim. In comparison to Noachian-fan scaling relationship, the proportionality constant has decreased from 2.82 to 0.92 which solidifies the previous statement. The new scaling relationship exponent is the same as the original scaling law's exponent, 0.97, showing that the size of catchment area is almost directly proportionate to the size of the fan area allowing for an interpretation that fluvial events may have occurred to transport the sediment during this period. From this analysis, alluvial fans show that young alluvial fan catchments formed during the Amazonian and Hesperian time periods generally have a stronger relationship to the alluvial fan area. This shows that all sediment within the catchment was transported to the basin to build the fan. However, there may be preservation bias on the fan and catchment that will need to be further investigated potentially due to wind-driven sediment transport processes during the more arid time periods.

5.2 Planetary-scale and local geomorphic setting variation

The Martian latitude variation is heavily due to elevation differences in the north and the south. As previously stated, the planet has a dichotomy boundary that separates the two latitudes. The northern lowlands, dichotomy boundary, and southern highlands were used as subsets to interpret new scaling relationships for fans found in craters or non-craters in each location. To begin, the northern lowlands contain $n_{fans} = 96$ fans found within craters (Figure 9a) and $n_{fans} = 1$ fan found in a non-cratered setting. The large number of fans found within craters in the northern hemisphere is confounding given that this latitude boundary is interpreted as an old ocean basin by previous literature due to the sheer lack of craters within this location. A scaling relationship was not shown for the single fan found within the non-crater setting. However, the scaling relationship gathered for fans in craters is $A_f = 0.99 * A_c^{0.97}$ (Figure 9a). The proportionality constant, 0.99, shows that the alluvial fans within the northern lowlands was potentially formed in fluvial induced scenarios rather than mass wasting events. The exponent of 0.97 shows that the catchment area size is almost directly proportional to the fan area. Many large catchment areas in this subset do produce similarly large fan areas (Figure 9a). This discovery is close to the original in-crater scaling relationship found by Morgan et al. (2022).

The dichotomy boundary, which is situated on the outer edge of the Tharsis bulge and Valles Marineris, represents a transitional region characterized by intermediate elevations lying between the low elevations to the north and the high elevations to the south. 338 alluvial fans were found within this boundary, $n_{fans} = 236$ of which are located within a cratered setting and $n_{fans} = 102$ are in non-craters. The scaling relationship for fans in craters within the dichotomy boundary is $A_f = 1.90 * A_c^{0.68}$ (Figure 9b). The proportionality constant of 1.90 suggests a wet climate and an intermediate level of erosional efficiency. Fans within this region contain a lower exponent value of 0.68, which consists of small catchment areas producing relatively large fans (Figure 9b). The

interpreted potential climate that produced these fans may consist of low frequency flooding events for such large fans to occur (Blair & McPherson, 1994; Dorn, 1994; Giles, 2010; Adrian Harvey, 1997a). For fans built in non-cratered systems in this region, the scaling relationship is: $A_f = 5.98 * A_c^{0.42}$ (Figure 9c). Compared to the original scaling relationship for fans found in non-craters is $A_f = 5.37 * A_c^{0.50}$, this relationship demonstrates a high proportionality constant with a small exponent exhibiting a low ratio for fan area and catchment area. These characteristics suggest an interpreted predominantly wet climate environment, possibly leading to mass wasting events, as indicated by the smaller catchment areas generating larger fan areas (Dorn, 1994; Adrian Harvey, 1997a; Kochel, 1990).

The southern highlands are characterized by being heavily cratered and contains $n_{fans} = 947$ alluvial fans. Within this region, $n_{fans} = 736$ fans are found in a cratered geologic setting. The scaling relationship observed these fans is: $A_f = 1.45 * A_c^{0.76}$ (Figure 9d). This subset of fans exhibits an intermediate proportionality constant and exponent suggesting that alluvial fans formed in craters in this region may have originated from fluvial transport processes. While smaller catchments tend to generate equally small fans, they also possess the potential to produce larger fans, possibly due to the presence of loose sediment around the crater rim. 211 alluvial fans were identified within non-cratered systems in the same region. The new scaling relationship found for this subset is $A_f = 5.37 * A_c^{0.50}$ which is very similar to the relationship for fans in non-craters in the dichotomy boundary and is the same power law scaling relationship as the original non-crater overall subset (Figure 4, 9e). This trend suggests that these fans may have formed potentially in a humid climate, where low-frequency flooding events trigger mass wasting processes within the catchment, leading to deposition in the respective basin. Within this subset, smaller catchments produce relatively larger fan areas. This analysis further implies that the systematic variation between fans in craters and non-craters extends geographically as shown by Morgan et al. (2022).

Based on the comparisons of the subsets listed above, I speculate that fans hosted in non-craters were formed by fluvial processes in a relatively wet climate. This model is supported by observations for fans formed in Noachian-aged craters given that the proportionality constant in this scenario is the highest for all cratered fans and the lowest exponent ratio for fan area to catchment area. To further investigate why there is a systematic difference in ratio and proportionality constant for fans in craters and non-craters, I have explored two possible factors that can affect the variations: basin geometry and catchment relief.

5.3 Basin geometry implications on the ratio of fan area versus catchment area

When examining the influence of basin geometry on fan size, pairs 1, 2, and 5 consistently demonstrated results aligning with my hypothesis showing that the in-crater geomorphic setting generally exhibits a steep slope on the crater wall and a steep slope of the fan in comparison to the non-crater scenario (Figure 6, 10, 11, 14). Fan profiles exhibit a concave geometry; however, it was not possible to consistently interpret the basin shape solely using the approach taken shown in study sites Non-crater MC-23-5, Crater 11-0-00122-2, and Non-crater MC-13-4 (Figures 10d, 12c, 14d). In pair 3, the fan in Non-crater MC-18-6 features a steeper profile compared to its crater counterpart, possibly formed by mass wasting events due to a smaller catchment located on a valley wall. Likewise, in pair 4, the alluvial fan in Non-crater MC-0-91 displays a long, sinuous catchment shape illustrating that my hypothesis was incorrect for pairs 3 and 4 (Figure 12, 13). While basin geometry alludes to correct theories that may affect the scaling relationship between fan area and catchment area, it does not offer a comprehensive understanding of the variation. Ideally, further analysis would involve examining fan geometry in three-dimensional space. For

terrestrial alluvial fans, gathering grain sizes enables geomorphologists gather evidence for potential paleoclimate theories (D'Arcy et al., 2017; Dorn, 1994; A. Harvey, 1990; Kochel, 1990). Investigating the depth of the subsurface and grain sizes of alluvial fans in both cratered and non-cratered settings would enhance our understanding of Mars' paleoclimate transitions. Future missions could involve examining fan geometry beneath the surface using the Mars Advanced Radar of Subsurface and Ionosphere Sounding (MARSIS) to send radar through the surface to characterize basin geometry more effectively than can be done from topography alone (Jordan et al., 2009). Alternatively, high-resolution seismic reflection could be used to gather profiles of the alluvial fan to see bedrock thickness and sediment accumulation to better understand the factors that may alter the proportionality constant for fans in craters and non-craters (Maraio et al., 2018).

5.4 Catchment relief implications on the ratio of fan area versus catchment area

Among the five pairs examined, pairs 2 through 5 consistently demonstrate that catchments exhibit low relief for fans within craters and high relief in non-cratered settings (Figure 15). This aligns with my initial hypothesis suggesting that catchments in non-cratered settings will tend to be steeper as they are typically found along valley walls. Notably, many of the catchments associated with fans within craters in this analysis displayed sinuous, channel-like shapes and were situated on the outer crater surface rather than the crater rim. The analysis further supports Morgan et al. (2022)'s original scaling relationship variation for fans in craters and non-craters by showing consistent low catchment relief in craters. Fans found in craters in the original dataset showed that catchment area was a good indicator for fan area displaying that all the sediment within the catchment at the crater rim moved down slope into the basin to build the fan. Fans in non-craters show that catchment area is a weak indicator for fan size meaning that the fan area varies based on the sediment transport processes occurring in the catchment. This analysis is important for showing the variation between understanding how terrestrial alluvial fans are built versus alluvial fan building on Mars. However, the relationship between fan area and catchment relief is inconclusive given that the pairs alter which geomorphic setting produces the larger fan per pair.

6. Conclusions

Recent literature suggests that Mars sustained a warm and wet climate intermittently through much of its history (Holo et al., 2021, 2021; Kite, 2019; Kite et al., 2017; Morgan et al., 2022; Wilson et al., 2021). Possible sources for surface water in this wet climate include snowmelt or rainfall events (Holo et al., 2021; Morgan et al., 2022; Wilson et al., 2021). In conclusion, the scaling relationships observed in alluvial fans are linked to the geomorphic context in which they form. During the Noachian period, catchment area is not proportionately linked to fan area, however, the alluvial fans formed during the Hesperian and Amazonian period exhibit almost linear relationships between the two alluding to a differing climate between the three periods. This trend extends to fans within cratered regions of the northern lowlands and southern highlands, suggesting similar transport processes for fans built in craters. Alternatively, fans hosted in craters in the dichotomy boundary display a low fan area to catchment area ratio exponent (below 0.7) and a high proportionality constant relative to the original constant found by Morgan et al. (2022) suggesting a weaker relationship between fan area and catchment area. Similarly, fans in non-cratered regions of the dichotomy boundary and southern highlands have large proportionality constants and low exponent values akin to the non-crater scaling relationship found by Morgan et al. (2022). To summarize, the scaling relationship between fan area and catchment area for alluvial fans show systematic variations via fan age and latitude. Catchments, from young alluvial fans

formed during the Hesperian and Amazonian period as well as for all fans in-craters geographically, are strong indicators for fan area. This analysis, coupled with further investigations such as gathering grain size evidence to better understand the processes that formed the fans (i.e., fluvial processes or mass wasting events), can be used to infer climatic transitions during different geologic periods and within different planetary-scale geomorphic settings.

Further analysis of the five pairs of study sites revealed that catchment relief alone does not consistently influence scaling variation given that fan area is not inherently correlated with catchment relief for fans in craters or non-craters. With this in mind, crater rim catchments tend to exhibit lower relief compared to non-cratered settings which is shown from the original dataset produced by Morgan et al. (2022). The observed differences in scaling relationships may be related to differences in alluvial fan slope based on topographic profiles of the fan surface. Further work is needed to better determine basin geometry for these alluvial fans, as this key variable was not consistently measurable from orbital data. In summary, the alluvial fan geometries considered here showed systematic differences with respect to local geomorphic setting (crater versus non-crater), large-scale geomorphic setting (northern lowlands versus dichotomy boundary versus southern highlands), and fan age. An important objective for future work is to distinguish whether these differences in geometry were the result of geologic conditions (e.g., basin geometry) versus differences in climate.

7. References

- Blair, T. C., & McPherson, J. G. (1994). Alluvial fans and their natural distinction from rivers based on morphology, hydraulic processes, sedimentary processes, and facies assemblages. *Journal of Sedimentary Research*, 64(3a), 450–489. <https://doi.org/10.1306/D4267DDE-2B26-11D7-8648000102C1865D>
- Bull, W. B. (1963). Alluvial fan deposits in western Fresno County, California. *The Journal of Geology*, 71(2), 243–251. <https://doi.org/10.1086/626896>
- Bull, W. B. (1977). The alluvial-fan environment. *Progress in Physical Geography: Earth and Environment*, 1(2), 222–270. <https://doi.org/10.1177/030913337700100202>
- Chen, J., Wan, G., Zhang, D. D., Zhang, F., & Huang, R. (2004). Environmental records of lacustrine sediments in different time scales: Sediment grain size as an example. *Science in China Series D: Earth Sciences*, 47(10), 954–960. <https://doi.org/10.1360/03yd0160>
- Christensen, P. R., Jakosky, B. M., Kieffer, H. H., Malin, M. C., McSween, H. Y., Nealon, K., et al. (2004). The Thermal Emission Imaging System (THEMIS) for the Mars 2001 Odyssey Mission. *Space Science Reviews*, 110(1), 85–130. <https://doi.org/10.1023/B:SPAC.0000021008.16305.94>
- D’Arcy, M., Whittaker, A. C., & Roda-Boluda, D. C. (2017). Measuring alluvial fan sensitivity to past climate changes using a self-similarity approach to grain-size fining, Death Valley, California. *Sedimentology*, 64(2), 388–424. <https://doi.org/10.1111/sed.12308>
- Di Achille, G., & Hynek, B. M. (2010). Ancient ocean on Mars supported by global distribution of deltas and valleys. *Nature Geoscience*, 3(7), 459–463. <https://doi.org/10.1038/ngeo891>
- Dietrich, W. E., Palucis, M. C., Williams, R. M. E., Lewis, K. W., Rivera-Hernandez, F., & Sumner, D. Y. (2017). Fluvial gravels on Mars: Analysis and implications. In D. Tsutsumi & J. B. Laronne (Eds.), *Gravel-Bed Rivers* (1st ed., pp. 755–783). Wiley. <https://doi.org/10.1002/9781118971437.ch28>
- Dorn, R. I. (1994). The role of climatic change in alluvial fan development. In A. D. Abrahams & A. J. Parsons (Eds.), *Geomorphology of Desert Environments* (pp. 593–615). Dordrecht: Springer Netherlands. https://doi.org/10.1007/978-94-015-8254-4_23
- Giles, P. T. (2010). Investigating the use of alluvial fan volume to represent fan size in morphometric studies. *Geomorphology*, 121(3–4), 317–328. <https://doi.org/10.1016/j.geomorph.2010.05.001>
- Grant, J. A., & Wilson, S. A. (2011). Late alluvial fan formation in southern Margaritifer Terra, Mars. *Geophysical Research Letters*, 38(8). <https://doi.org/10.1029/2011GL046844>
- Hartmann, W. K. (2005). Martian cratering 8: Isochron refinement and the chronology of Mars. *Icarus*, 174(2), 294–320. <https://doi.org/10.1016/j.icarus.2004.11.023>
- Harvey, A. (1990). Factors influencing Quaternary alluvial fan development in southeast Spain. In *Alluvial fans: a field approach* (p. 22). John Wiley and Sons Ltd.
- Harvey, Adrian. (1997a). The role of alluvial fans in arid zone fluvial systems. In *Arid zone geomorphology: Process, form, and changes in drylands* (p. 28). Wiley.
- Harvey, Adrian. (1997b). The role of alluvial fans in arid zone fluvial systems. *Wiley*, 28.
- Holo, S. J., Kite, E. S., Wilson, S. A., & Morgan, A. M. (2021). The timing of alluvial fan formation on Mars. *The Planetary Science Journal*, 2(5), 210. <https://doi.org/10.3847/PSJ/ac25ed>
- Hynek, B. M., Beach, M., & Hoke, M. R. T. (2010). Updated global map of Martian valley networks and implications for climate and hydrologic processes. *Journal of Geophysical Research: Planets*, 115(E9). <https://doi.org/10.1029/2009JE003548>

- Jakosky, B. M. (2021). Atmospheric loss to space and the history of water on Mars. *Annual Review of Earth and Planetary Sciences*, 49(1), 71–93. <https://doi.org/10.1146/annurev-earth-062420-052845>
- Jordan, R., Picardi, G., Plaut, J., Wheeler, K., Kirchner, D., Safaeinili, A., et al. (2009). The Mars express MARSIS sounder instrument. *Planetary and Space Science*, 57(14), 1975–1986. <https://doi.org/10.1016/j.pss.2009.09.016>
- Kite, E. S. (2019). Geologic constraints on early Mars climate. *Space Science Reviews*, 215(1), 10. <https://doi.org/10.1007/s11214-018-0575-5>
- Kite, E. S., Sneed, J., Mayer, D. P., & Wilson, S. A. (2017). Persistent or repeated surface habitability on Mars during the late Hesperian - Amazonian. *Geophysical Research Letters*, 44(9), 3991–3999. <https://doi.org/10.1002/2017GL072660>
- Kochel, R. C. (1990). Humid fans of the Appalachian Mountains. In *Alluvial fans: A field approach* (p. 20). Wiley.
- Lecce, S. (1990). The alluvial fan problem. In *Alluvial fans: A field approach* (p. 21). John Wiley and Sons Ltd.
- Malin, M. C., Bell III, J. F., Cantor, B. A., Caplinger, M. A., Calvin, W. M., Clancy, R. T., et al. (2007). Context Camera investigation on board the Mars Reconnaissance Orbiter. *Journal of Geophysical Research*, 112. <https://doi.org/10.1029/2006JE002808>.
- Maraio, S., Bruno, P. P. G., Picotti, V., Mair, V., & Brardinoni, F. (2018). High-resolution seismic imaging of debris-flow fans, alluvial valley fills and hosting bedrock geometry in Vinschgau/Val Venosta, Eastern Italian Alps. *Journal of Applied Geophysics*, 157, 61–72. <https://doi.org/10.1016/j.jappgeo.2018.07.001>
- Michael, G. G., & Neukum, G. (2010). Planetary surface dating from crater size–frequency distribution measurements: Partial resurfacing events and statistical age uncertainty. *Earth and Planetary Science Letters*, 294(3), 223–229. <https://doi.org/10.1016/j.epsl.2009.12.041>
- Michael, G. G., Kneissl, T., & Neesemann, A. (2016). Planetary surface dating from crater size–frequency distribution measurements: Poisson timing analysis. *Icarus*, 277, 279–285. <https://doi.org/10.1016/j.icarus.2016.05.019>
- Milliken, R. E., Grotzinger, J. P., & Thomson, B. J. (2010). Paleoclimate of Mars as captured by the stratigraphic record in Gale Crater. *Geophysical Research Letters*, 37(4). <https://doi.org/10.1029/2009GL041870>
- Mondro, C. A., Moersch, J. E., & Fedo, C. M. (2023). An updated global survey of alluvial fans on Mars: Distinguishing alluvial fans from other fan-shaped features through morphologic characterization. *Icarus*, 389, 115238. <https://doi.org/10.1016/j.icarus.2022.115238>
- Moore, J. M. (2005). Large alluvial fans on Mars. *Journal of Geophysical Research*, 110(E4), E04005. <https://doi.org/10.1029/2004JE002352>
- Moore, J. M., Howard, A. D., Dietrich, W. E., & Schenk, P. M. (2003). Martian layered fluvial deposits: Implications for Noachian climate scenarios. *Geophysical Research Letters*, 30(24). <https://doi.org/10.1029/2003GL019002>
- Morgan, A. M., Howard, A. D., Hopley, D. E. J., Moore, J. M., Dietrich, W. E., Williams, R. M. E., et al. (2014). Sedimentology and climatic environment of alluvial fans in the martian Saheki crater and a comparison with terrestrial fans in the Atacama Desert. *Icarus*, 229, 131–156. <https://doi.org/10.1016/j.icarus.2013.11.007>

- Morgan, A. M., Wilson, S. A., & Howard, A. D. (2022). The global distribution and morphologic characteristics of fan-shaped sedimentary landforms on Mars. *Icarus*, 385, 115137. <https://doi.org/10.1016/j.icarus.2022.115137>
- Pan, L., Ehlmann, B. L., Carter, J., & Ernst, C. M. (2017). The stratigraphy and history of Mars' northern lowlands through mineralogy of impact craters: A comprehensive survey. *Journal of Geophysical Research: Planets*, 122(9), 1824–1854. <https://doi.org/10.1002/2017JE005276>
- Rachocki, A., & Church, M. (1990). *Alluvial fans: a field approach*. John Wiley and Sons Ltd.
- Robbins, S. J., & Hynek, B. M. (2012). A new global database of Mars impact craters ≥ 1 km: 1. Database creation, properties, and parameters. *Journal of Geophysical Research: Planets*, 117(E5). <https://doi.org/10.1029/2011JE003966>
- Robinson, C. A. (1995). The crustal dichotomy of Mars. *Earth, Moon, and Planets*, 69(3), 249–269. <https://doi.org/10.1007/BF00643787>
- Smith, D. E., Zuber, M. T., Solomon, S. C., Phillips, R. J., Head, J. W., Garvin, J. B., et al. (1999). The global topography of Mars and implications for surface evolution. *Science*, 284(5419), 1495–1503. <https://doi.org/10.1126/science.284.5419.1495>
- Stock, J. D. (2013). Waters divided: A history of alluvial fan research and a view of its future. In *Treatise on Geomorphology* (pp. 680–722). Elsevier. <https://doi.org/10.1016/B978-0-12-818234-5.60043-3>
- Sundararajan, G., Roy, M., & Venkataraman, B. (1990). Erosion efficiency—a new parameter to characterize the dominant erosion micromechanism. *Wear*, 140(2), 369–381. [https://doi.org/10.1016/0043-1648\(90\)90096-S](https://doi.org/10.1016/0043-1648(90)90096-S)
- Tanaka, K. L., Robbins, S. J., Fortezzo, C. M., Skinner, J. A., & Hare, T. M. (2014). The digital global geologic map of Mars: Chronostratigraphic ages, topographic and crater morphologic characteristics, and updated resurfacing history. *Planetary and Space Science*, 95, 11–24. <https://doi.org/10.1016/j.pss.2013.03.006>
- Wilson, S. A., Morgan, A. M., Howard, A. D., & Grant, J. A. (2021). The global distribution of craters with alluvial fans and deltas on Mars. *Geophysical Research Letters*, 48(4). <https://doi.org/10.1029/2020GL091653>
- Wordsworth, R. D. (2016). The climate of early Mars. *Annual Review of Earth and Planetary Sciences*, 44(1), 381–408. <https://doi.org/10.1146/annurev-earth-060115-012355>

8. Figures

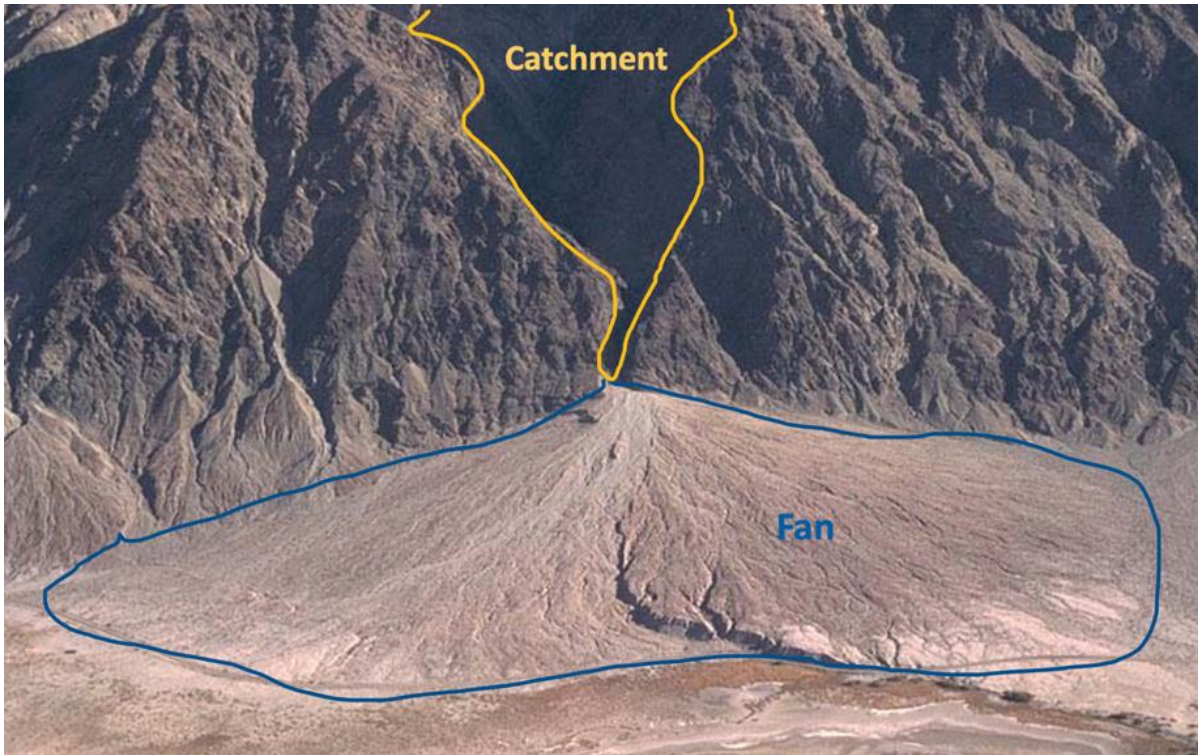


Figure 1. Classic example of a terrestrial alluvial fan found in Death Valley, CA near the Badwater Basin. The yellow line shows the extent of the catchment, and the blue line shows the extent of the fan.

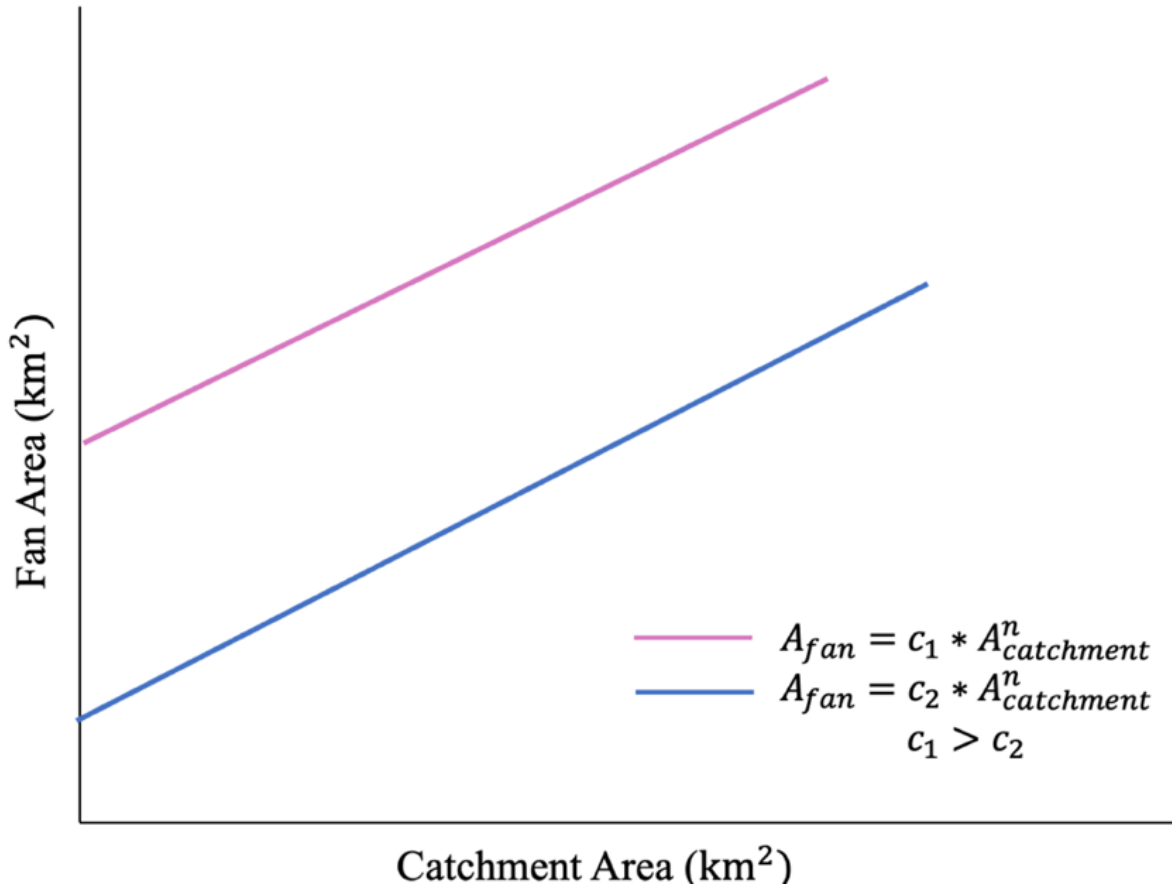


Figure 2. A plot showing the effects of the difference in proportionality constant causing the same catchment areas to produce differing fan areas. C_1 has a larger proportionality constant than C_2 allowing for the same size catchment areas to produce larger fans (Eq. 1). This scaling relationship is generally plotted on axes in log-scale.

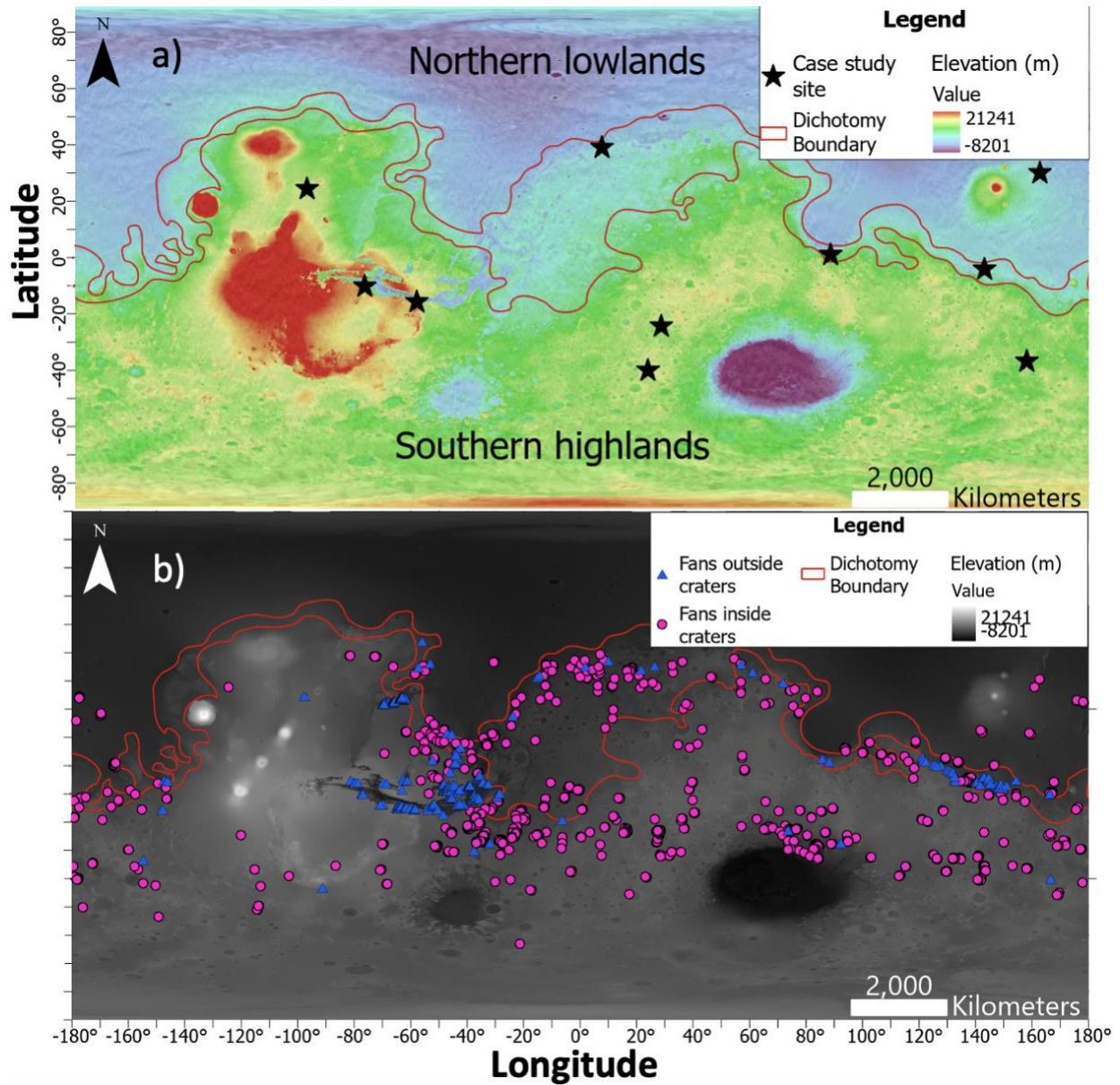


Figure 3. a) Global colorized elevation map of Mars showing the clear difference in elevation of the northern lowlands and the southern highlands and the dichotomy boundary that separates the two hemispheres. Case study sites have been depicted on this map (see methods). b) Grayscale MOLA DEM showing the locations of all alluvial fans studied by Morgan et al. (2022) globally (Morgan et al., 2022); modified from their Figure 3).

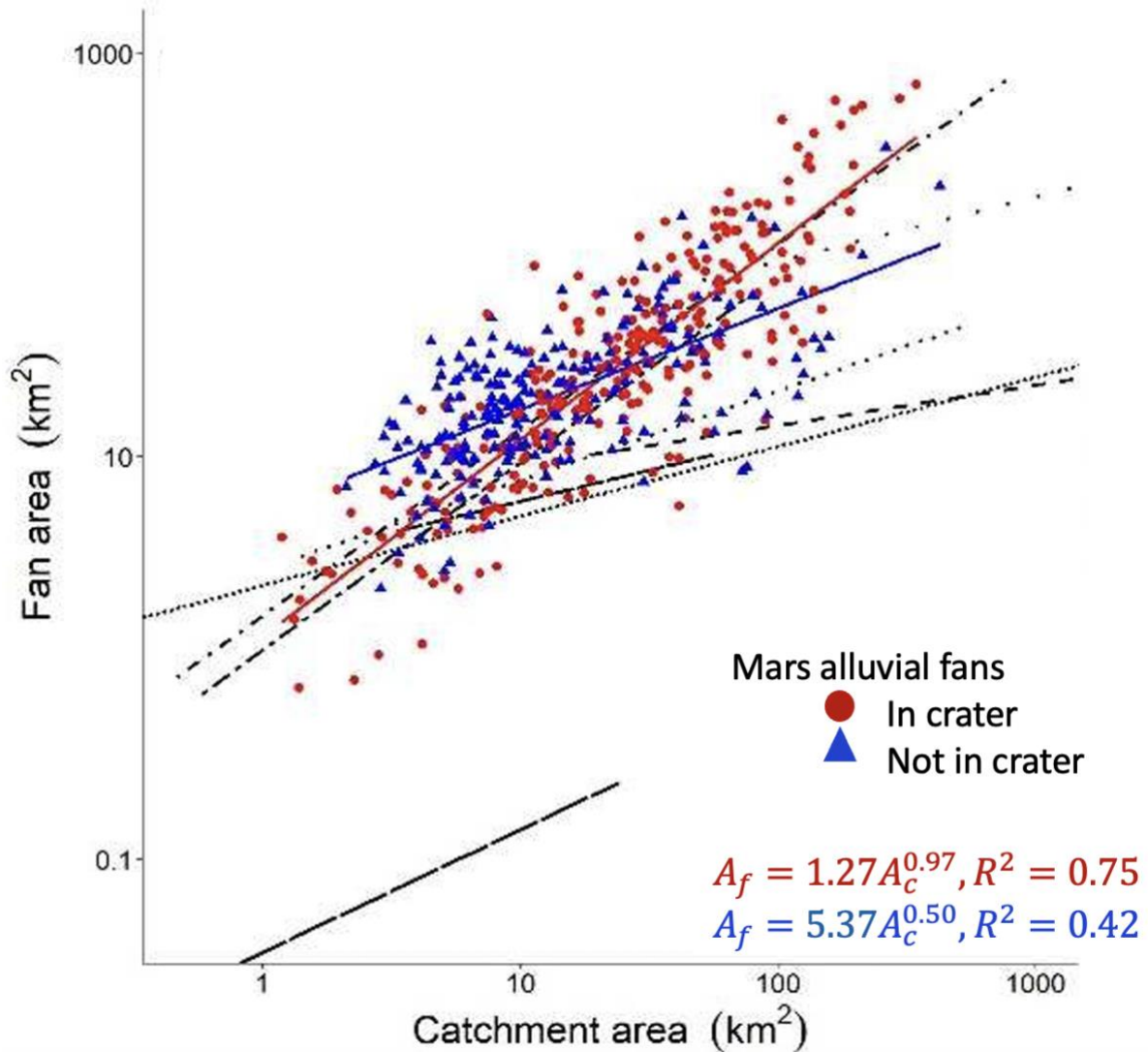


Figure 4. Plot of fan area versus catchment area for 1501 alluvial fans on Mars (Morgan et al., 2022; modified from their Figure 9a). The dashed lines in the plot represent terrestrial fans previously studied. Fans found in craters and not in craters were plotted in relation to heavily studied terrestrial fans in arid and humid regions. Martian fans found in craters portray a differing exponent and proportionality constant compared to the fans not located in craters.

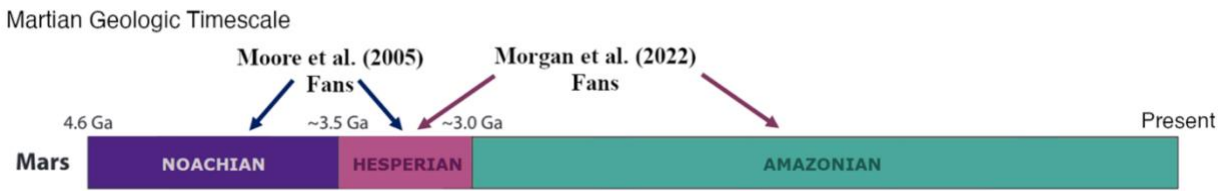


Figure 5. The geologic time scale showing the relative ages of fans examined by Moore et al. (2005) and Morgan et al. (2022) (Wordsworth, 2016; modified from their Figure 2).

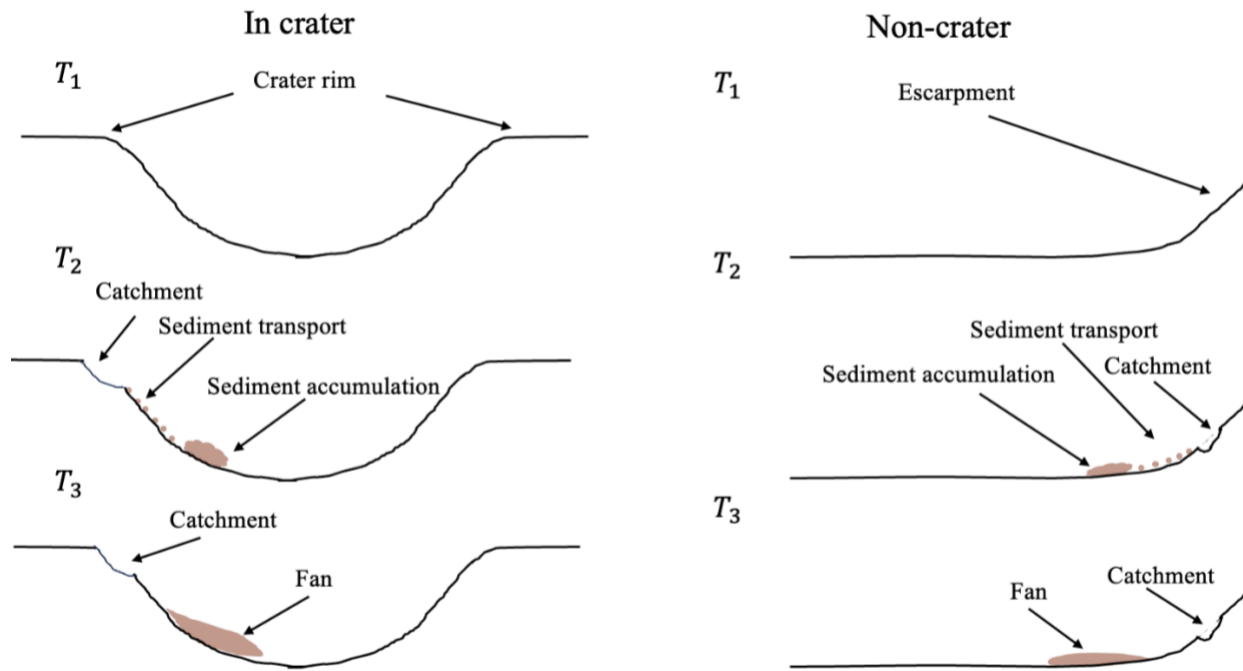


Figure 6. Time series schematic depicting how fans are built from sediment accumulation in a cratered geomorphic setting as well as a non-crater geomorphic setting. The fans hosted in craters have a designated catchment at the crater rim moving sediment down a steep slope that forms a vertically built alluvial fan. A fan hosted in a non-crater region will have its catchment at the escarpment and have a more tabular shape.

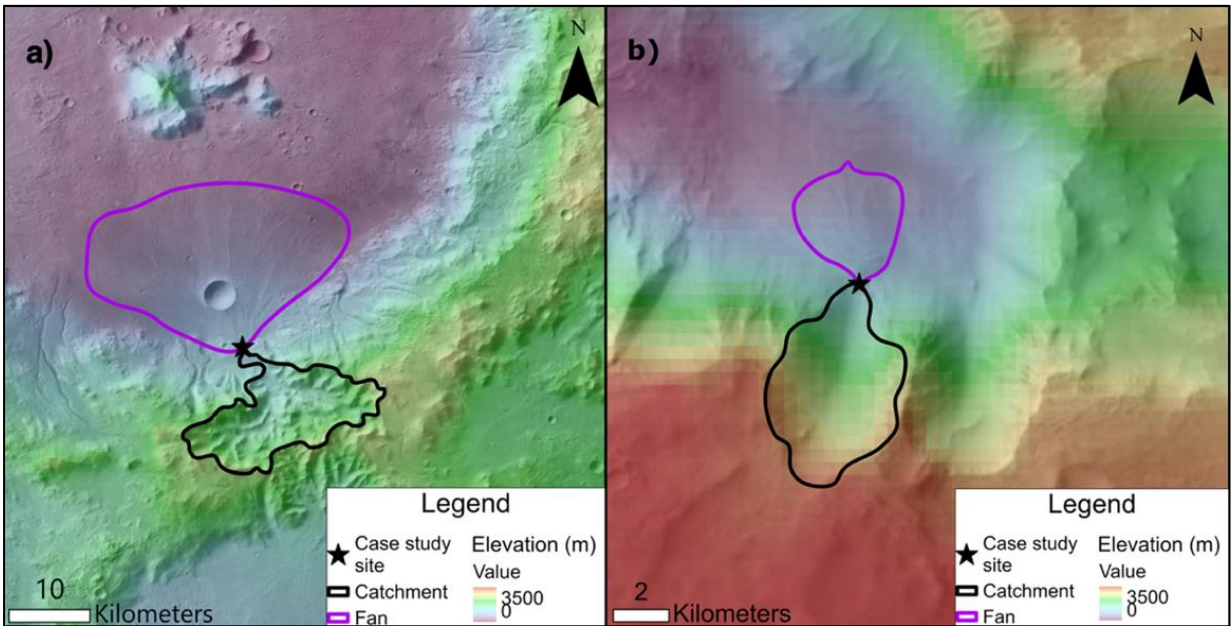


Figure 7. a) Elevation map showing an example in crater fan and its respective catchment for a study site depicted in table 1 using the Morgan et al. (2022) database. The purple polygon shows the extent of the fan mapped by using contour lines and the black line shows the extent of the can's catchment (28.1° E, 23.9° S). b) Elevation map showing an example non-crater fan and its respective catchment for a study site depicted in table 1 using the Morgan et al. (2022) database. The purple polygon shows the extent of the fan mapped by using contour lines and the black line shows the extent of the can's catchment (58.6° W, 15.3° S).

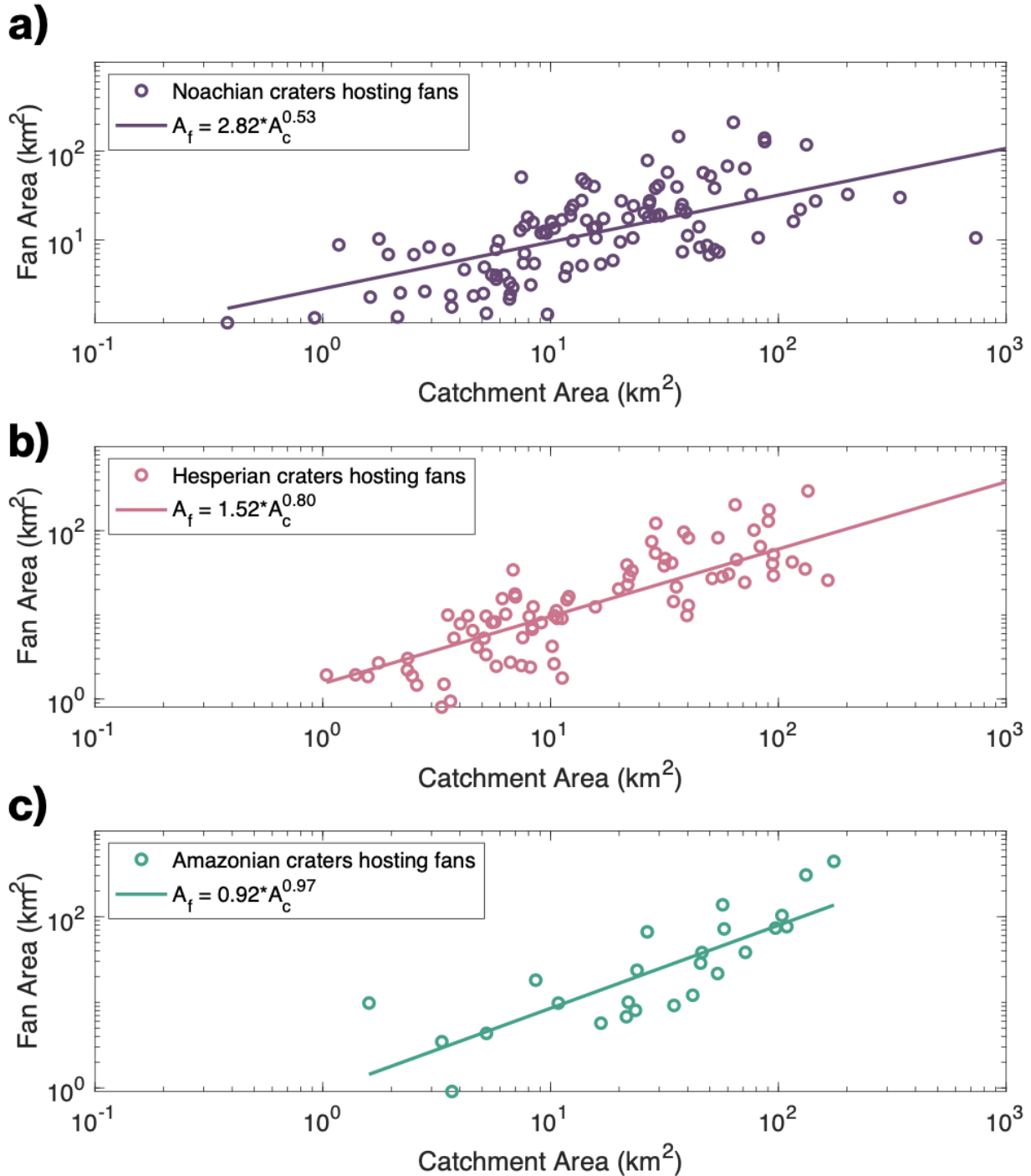


Figure 8. Fan area versus catchment area log-log plot for 219 Martian alluvial fans (Morgan et al., 2022; modified from their Figure 9a). The fans plotted are only found within Martian craters due to fan ages being based on crater counting capabilities explained by Morgan et al. (2022). Each temporal subset is accompanied by a corresponding trendline, illustrating distinct ratios through exponents and proportionality constants of fan area to catchment area. a) Purple markers represent fans formed during the Noachian Period (4.1 to 3.7 billion years ago) ($n= 111$). b) Pink markers signify fans from the Hesperian Period (3.7 to 3 billion years ago) ($n= 83$). c) Teal markers denote fans originating in the Amazonian Period (3 billion years to the present) ($n= 25$).

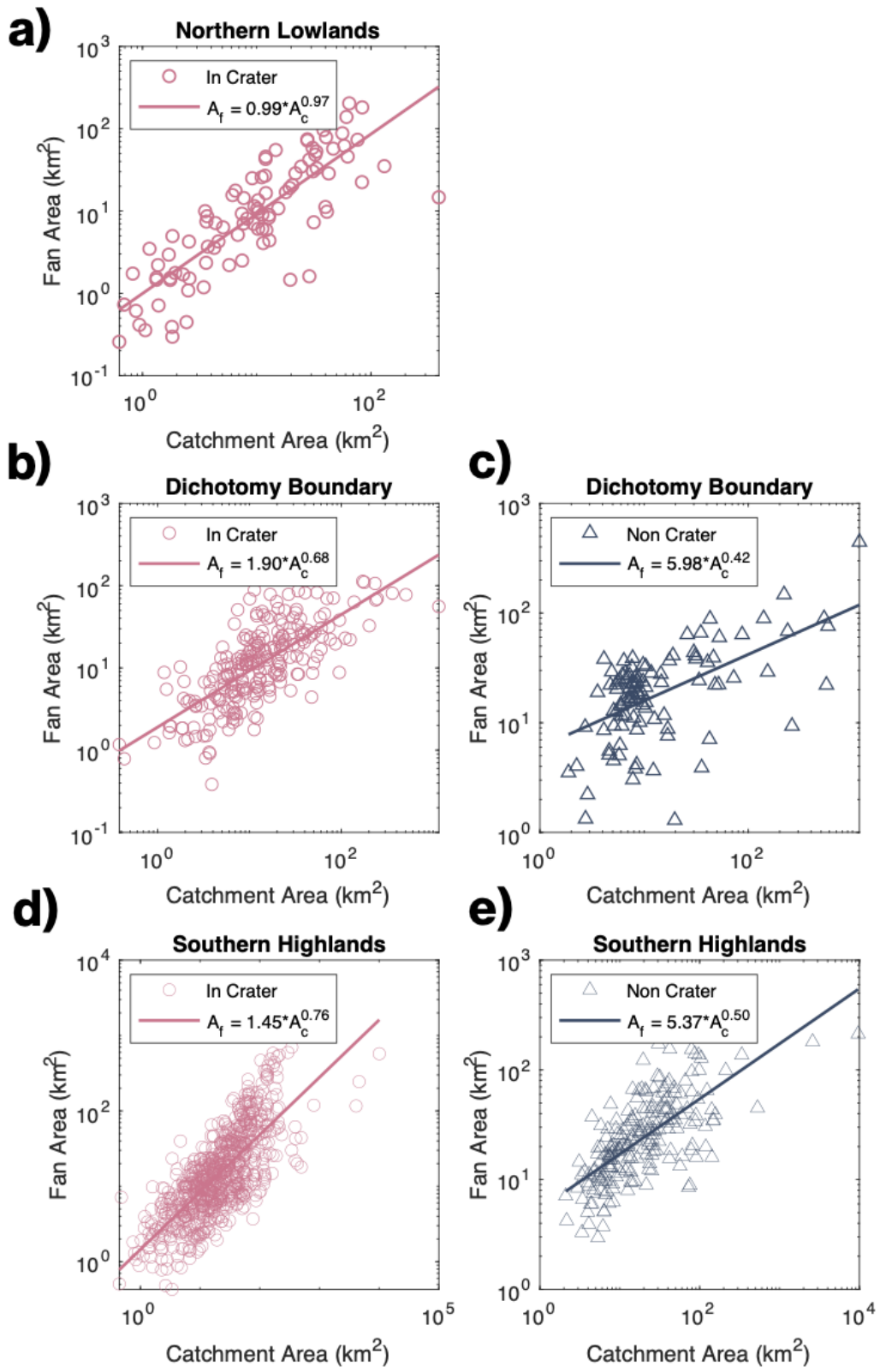


Figure 9 (caption next page)

Figure 9. Fan area versus catchment area log-log plot for $n=97$ Martian alluvial fans found within the northern lowlands, $n=338$ Martian alluvial fans found within the dichotomy boundary, and $n=947$ fans found within the southern highlands (Morgan et al., 2022; modified from their Figure 9a). a) $n=96$ fans have been discovered in cratered geomorphic settings and $n=1$ fan was found in a non-cratered geomorphic setting (not graphed). b) $n=236$ fans have been discovered in cratered geomorphic settings. c) $n=102$ fans have been discovered in non-cratered geomorphic settings. d) $n=736$ fans have been discovered in cratered geomorphic settings and e) $n=11$ fans have been discovered in non-cratered geomorphic settings. Each spatial subset is accompanied by a corresponding trendline, illustrating distinct ratios through exponents and proportionality constants of fan area to catchment area.

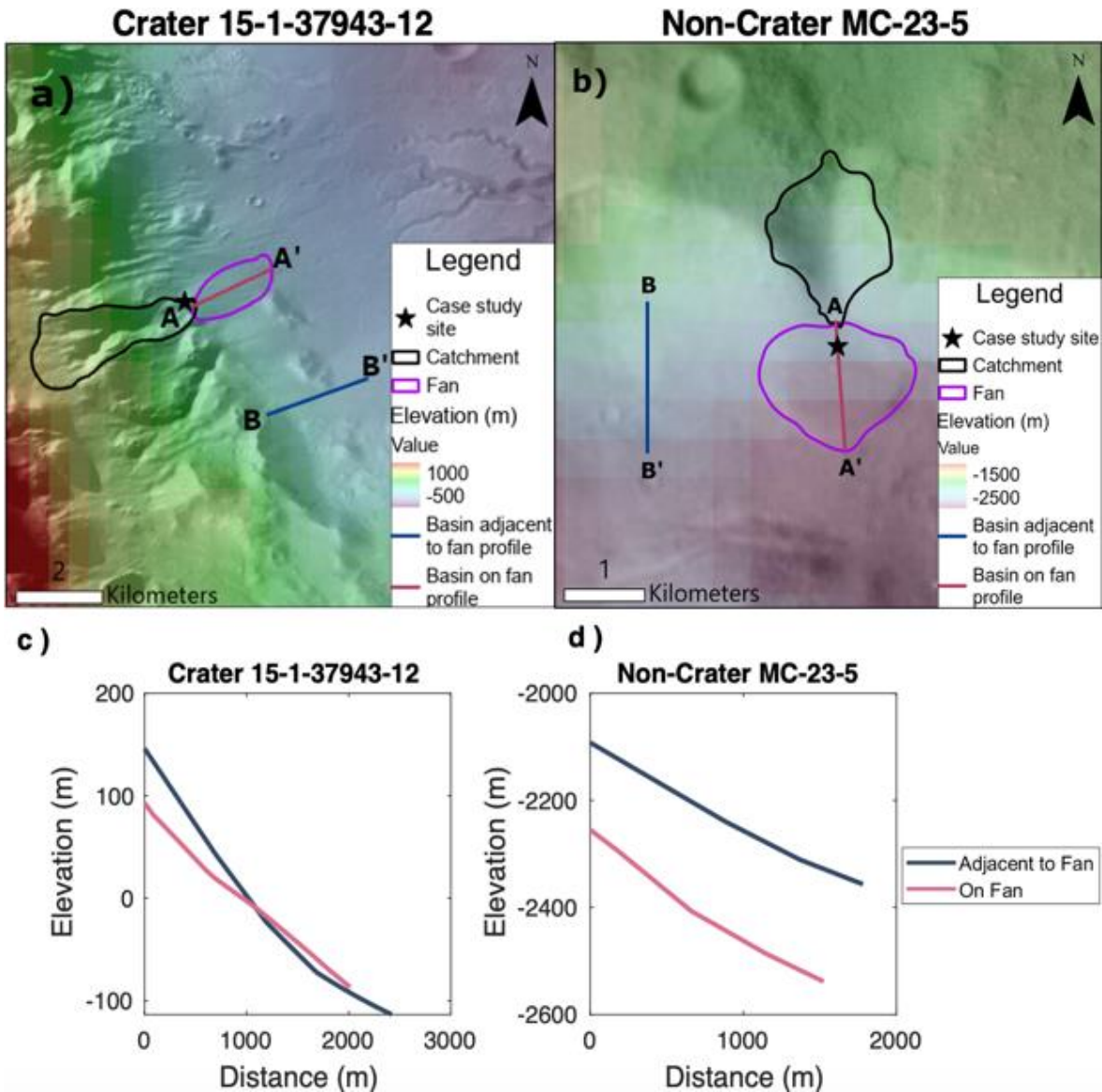


Figure 10. Pair 1 showing the elevation map with the fan and catchment marked and its longitudinal profile. All crater and non-crater names are derived from the Morgan et al. (2022) database. a) Crater 15-1-37943-12 with its on fan profile in pink labeled as A-A' and the profile of the basin adjacent to the fan in blue labeled as B-B' (157.9° E, 36.4° S). b) Non-crater MC-23-5 with its on fan profile in pink labeled as A-A' and the profile of the basin adjacent to the fan in blue labeled as B-B' (143.9° E, 3.7° S). c) The longitudinal profile for the crater fan profile in Figure 10a. The elevation profile from A-A' is shown in pink and the profile from B-B' is depicted in blue. d) The longitudinal profile for the crater fan profile in Figure 10b. The elevation profile from A-A' is shown in pink and the profile from B-B' is depicted in blue.

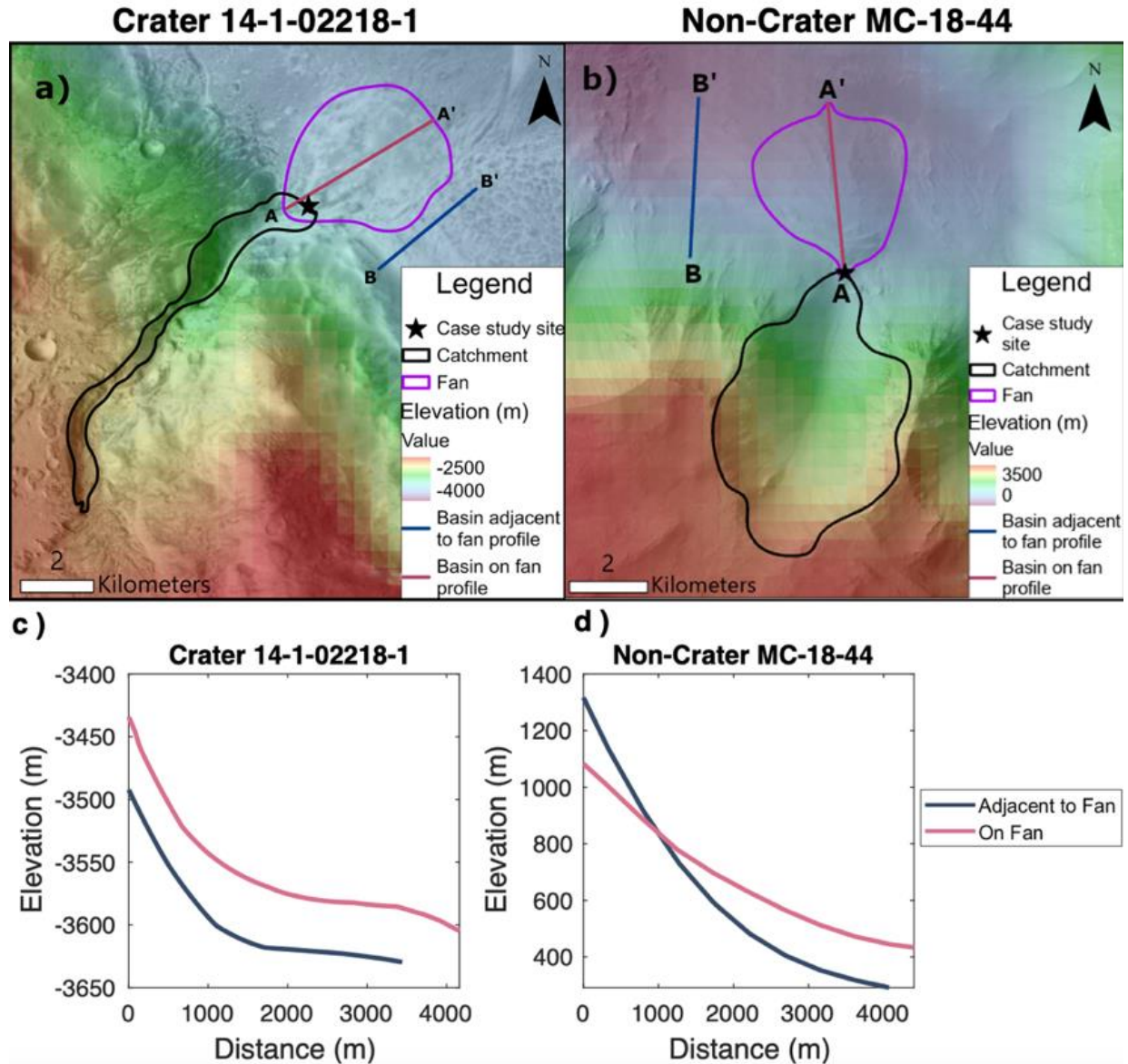


Figure 11. Pair 2 showing the elevation map with the fan and catchment marked and its longitudinal profile. All crater and non-crater names are derived from the Morgan et al. (2022) database. a) Crater 14-1-02218-1 with its on fan profile in pink labeled as A-A' and the profile of the basin adjacent to the fan in blue labeled as B-B' (162.6° E, 30.5° N). b) Non-crater MC-18-44 with its on fan profile in pink labeled as A-A' and the profile of the basin adjacent to the fan in blue labeled as B-B' (58.6° W, 15.3° S). c) The longitudinal profile for the crater fan profile in Figure 11a. The elevation profile from A-A' is shown in pink and the profile from B-B' is depicted in blue. d) The longitudinal profile for the crater fan profile in Figure 11b. The elevation profile from A-A' is shown in pink and the profile from B-B' is depicted in blue.

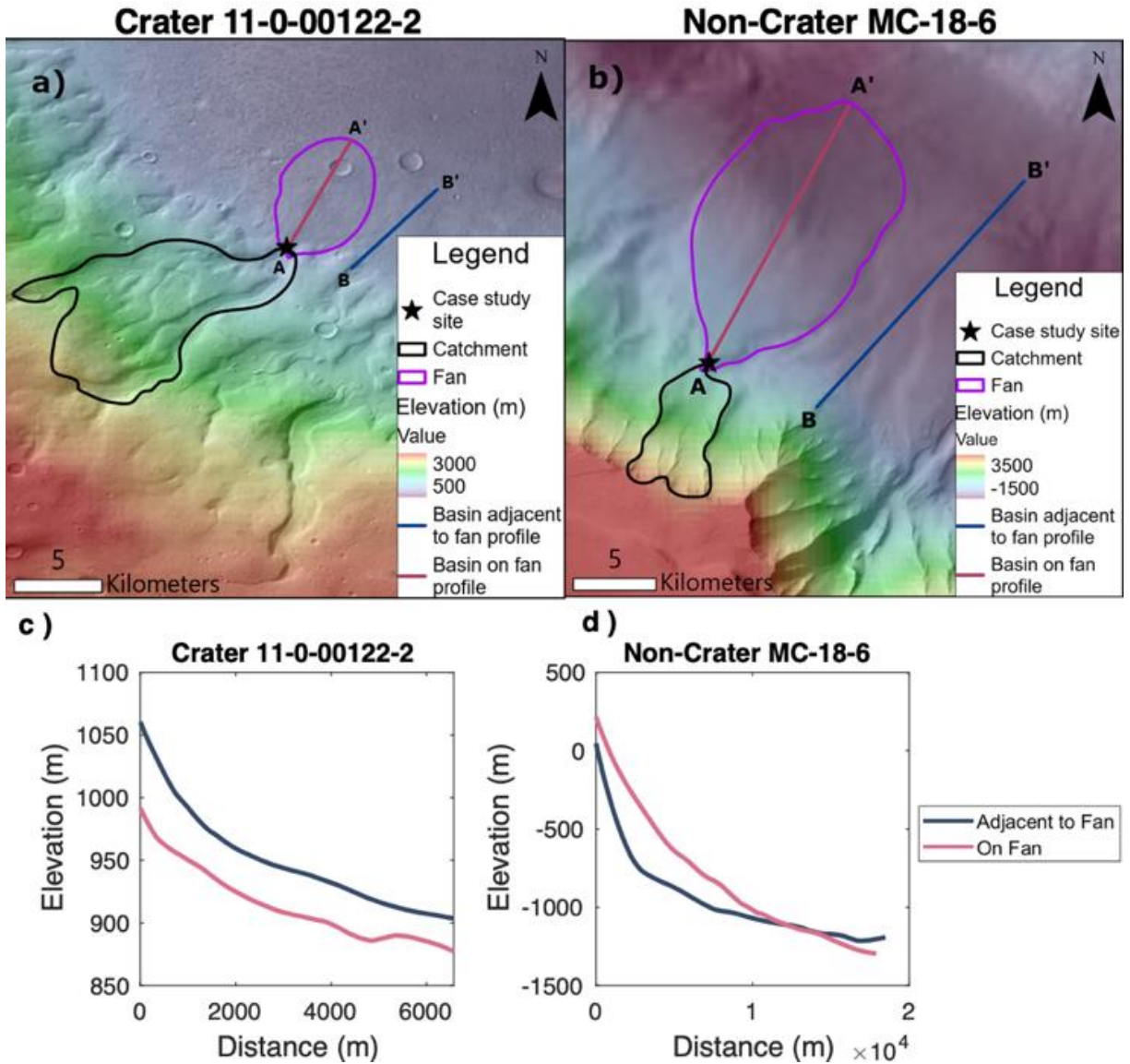


Figure 12. Pair 3 showing the elevation map with the fan and catchment marked and its longitudinal profile. All crater and non-crater names are derived from the Morgan et al. (2022) database. a) Crater 11-0-00122-2 with its on fan profile in pink labeled as A-A' and the profile of the basin adjacent to the fan in blue labeled as B-B' (23.4° E, 39.6° S). b) Non-crater MC-18-6 with its on fan profile in pink labeled as A-A' and the profile of the basin adjacent to the fan in blue labeled as B-B' (77.1° W, 9.8° S). c) The longitudinal profile for the crater fan profile in Figure 12a. The elevation profile from A-A' is shown in pink and the profile from B-B' is depicted in blue. d) The longitudinal profile for the crater fan profile in Figure 12b. The elevation profile from A-A' is shown in pink and the profile from B-B' is depicted in blue.

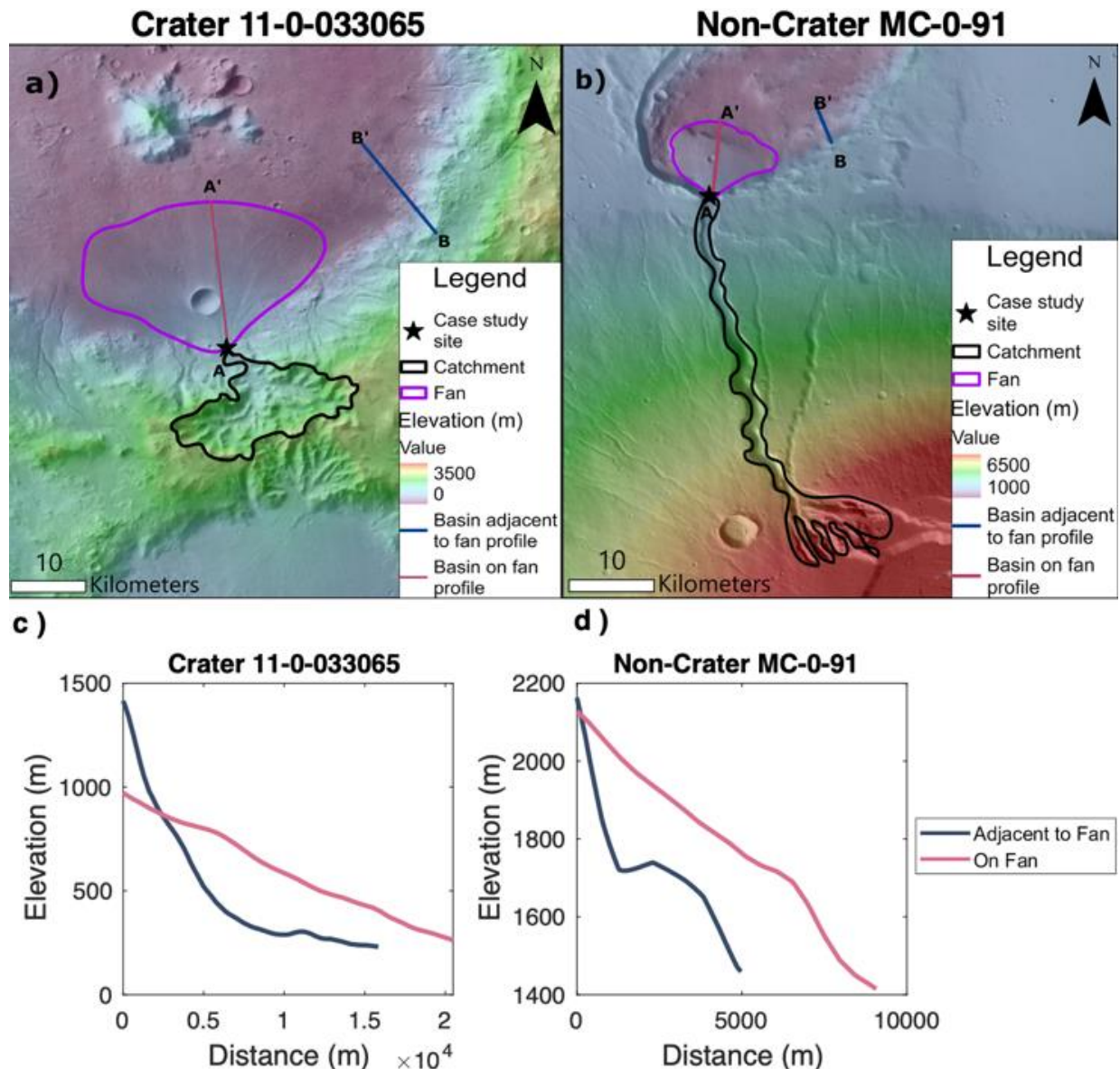


Figure 13. Pair 4 showing the elevation map with the fan and catchment marked and its longitudinal profile. All crater and non-crater names are derived from the Morgan et al. (2022) database. a) Crater 11-0-033065 with its on fan profile in pink labeled as A-A' and the profile of the basin adjacent to the fan in blue labeled as B-B' (28.1° E, 23.9° S). b) Non-crater MC-0-91 with its on fan profile in pink labeled as A-A' and the profile of the basin adjacent to the fan in blue labeled as B-B' (97.6° W, 24.8° N). c) The longitudinal profile for the crater fan profile in Figure 13a. The elevation profile from A-A' is shown in pink and the profile from B-B' is depicted in blue. d) The longitudinal profile for the crater fan profile in Figure 13b. The elevation profile from A-A' is shown in pink and the profile from B-B' is depicted in blue.

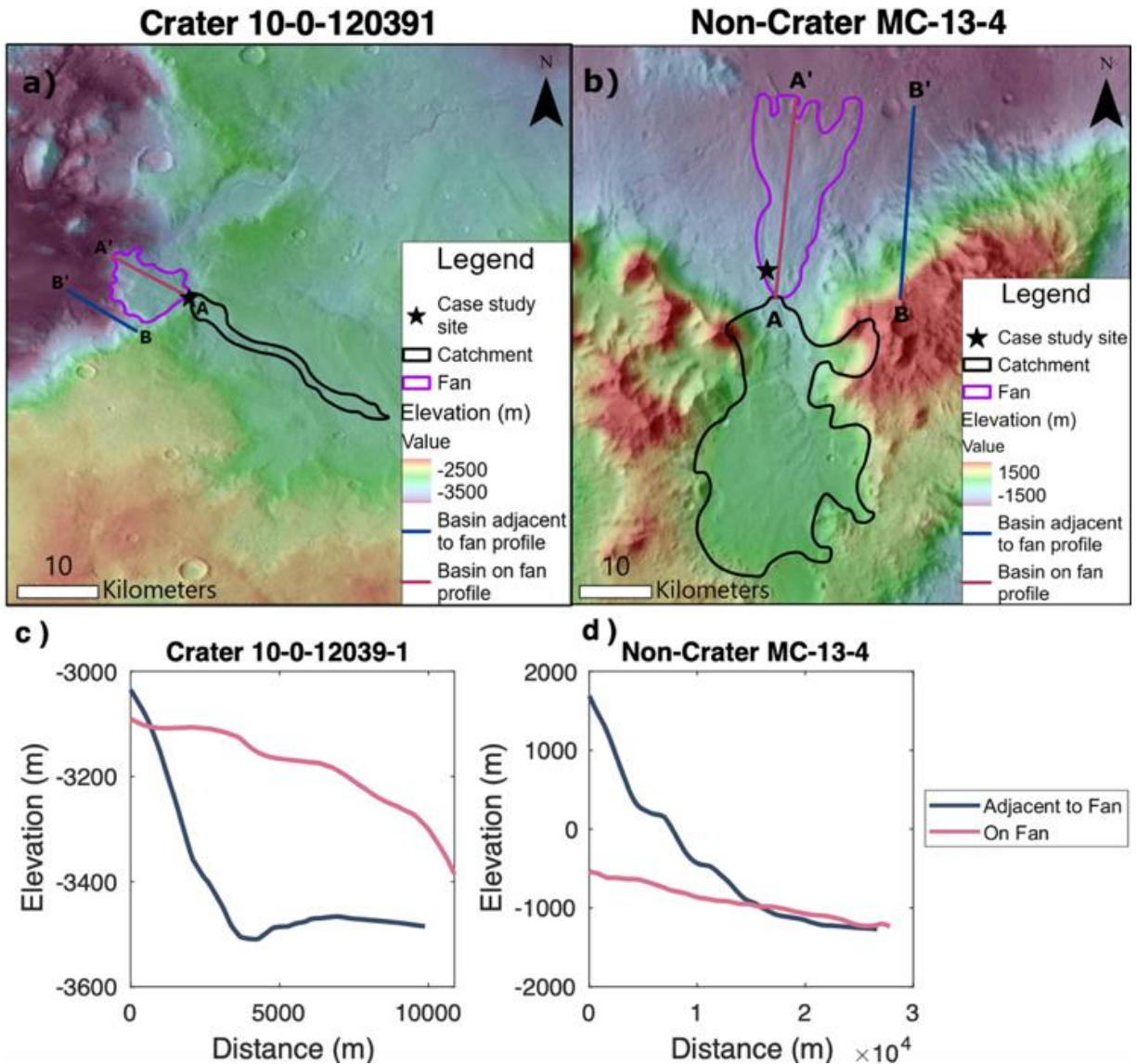


Figure 14. Pair 5 showing the elevation map with the fan and catchment marked and its longitudinal profile. All crater and non-crater names are derived from the Morgan et al. (2022) database. a) Crater 10-0-12039-1 with its on fan profile in pink labeled as A-A' and the profile of the basin adjacent to the fan in blue labeled as B-B' (7.1° E, 39.4° N). b) Non-crater MC-13-4 with its on fan profile in pink labeled as A-A' and the profile of the basin adjacent to the fan in blue labeled as B-B' (88.3° E, 1.4° N). c) The longitudinal profile for the crater fan profile in Figure 14a. The elevation profile from A-A' is shown in pink and the profile from B-B' is depicted in blue. d) The longitudinal profile for the crater fan profile in figure 14b. The elevation profile from A-A' is shown in pink and the profile from B-B' is depicted in blue.

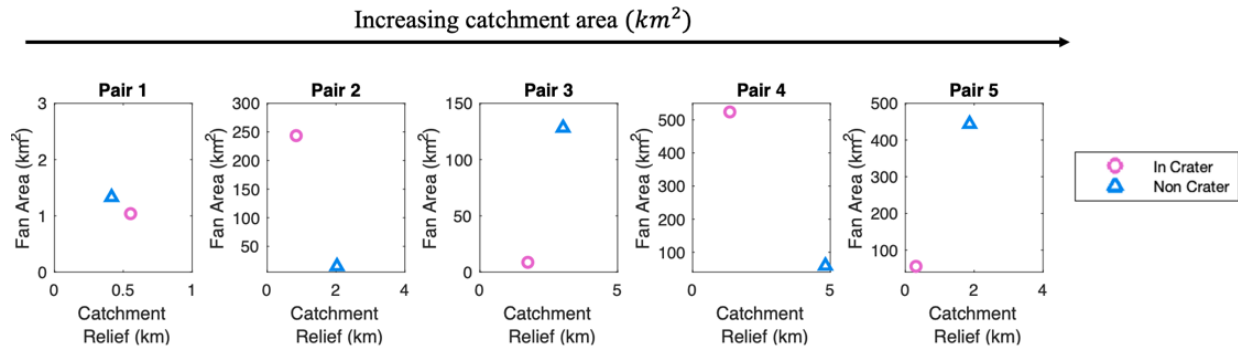


Figure 15. Five separate scatter plots showing the fan area versus catchment relief for all 5 pairs of study sites listed from smallest catchment area to largest catchment area right to left. Pink circles symbolize fan site inside of a crater and blue triangles represent the fan site in a non-crater. Values were gathered using the Morgan et al. (2022) database.